
Physics-Integrated Variational Autoencoders for Robust and Interpretable Generative Modeling

Naoya Takeishi^{1,2} Alexandros Kalousis¹

Abstract

Integrating physics models within machine learning holds considerable promise toward learning robust models with improved interpretability and abilities to extrapolate. In this work, we focus on the integration of incomplete physics models into deep generative models, variational autoencoders (VAEs) in particular. A key technical challenge is to strike a balance between the incomplete physics model and the learned components (i.e., neural nets) of the complete model, in order to ensure that the physics part is used in a meaningful manner. To this end, we propose a VAE architecture in which a part of the latent space is grounded by physics. We couple it with a set of regularizers that control the effect of the learned components and preserve the semantics of the physics-based latent variables as intended. We not only demonstrate generative performance improvements over a set of synthetic and real-world datasets, but we also show that we learn robust models that can consistently extrapolate beyond the training distribution in a meaningful manner. Moreover, we show that we can control the generative process in an interpretable manner.

1. Introduction

Data-driven modeling is often opposed to theory-driven modeling, yet their integration has also been recognized as an important approach and often called *gray-box* or *hybrid* modeling. In statistical machine learning, incorporation of knowledge of physics (in a broad sense; including biology, economics, engineering, etc.) has also been attracting attention. It holds considerable promise toward learning robust models with improved abilities to extrapolate beyond the distributions that they have been exposed to during training. Moreover, it can also bring significant benefits in terms of model interpretability.

While there are several approaches to integrating physics models into machine learning, a common challenge is to ensure an appropriate use of physics models. A careless design of models and learning can lead to an erratic behavior of the components meant to represent physics (e.g., with erroneous estimation of physics parameters), and eventually, the overall gray-box model just learns to ignore them. This is particularly the case when we bring together simplified or imperfect physics models with very expressive data-driven machine learning models such as deep neural networks. Such cases call for principled methods for striking an appropriate balance between physics and data-driven models to prevent the detrimental effects during learning.

Integration of physics models into machine learning has been considered in many contexts (see, e.g., surveys by Willard et al. (2020); von Rueden et al. (2020); and a short review in Section 4), but most existing studies focus on prediction or forecasting tasks and are not directly applicable to other tasks. More importantly, hardly any have addressed the careful orchestration of physics-based and data-driven components to avoid the detrimental effects. A notable exception is Le Guen et al. (2021), in which they proposed a method to harness the action of trainable components of a hybrid model of differential equations. Their method has been developed for dynamics forecasting and is limited to additive combinations of physics and trainable models.

In this work, we aim at the integration of (incomplete) physics models into deep generative models, variational autoencoders (VAEs, Kingma and Welling, 2014) in particular. In our VAE architecture, the decoder comprises physics-based components and trainable neural networks, and a part of the latent variables are semantically grounded to the parameters of the physics models. Such a VAE, if appropriately trained, is by construction interpretable. More importantly, since it can by construction capture the underlying physics, it will be robust in out-of-distribution regime and exhibit meaningful extrapolation properties.

The rest of the paper is structured as follows. We first give a general description of physics-integrated VAE models in Section 2, which subsumes various useful architectures as special cases. We then present a carefully orchestrated regularization approach in Section 3 for the meaningful use of

¹University of Applied Sciences and Arts Western Switzerland (HES-SO), Geneva, Switzerland ²RIKEN AIP, Tokyo, Japan. Correspondence to: Naoya Takeishi <naoya.takeishi@hesge.ch>.

the physics models and the preservation of the semantics of the latent variables. We empirically evaluate the proposed model on a set of synthetic and real world datasets in Section 5. We demonstrate that our model exhibits better generalization, and more importantly, can extrapolate robustly in out-of-distribution regime. In addition, we show how the direct access to the physics-grounded latent variables allows us to alter properties of generation meaningfully and explore counterfactual scenarios.

2. Physics-Integrated VAEs

Integrating physics models is attracting attention as a promising way to improve the performance and interpretability of machine learning models in tasks such as prediction (see Section 4). In this paper, we focus on the integration of physics models into variational autoencoders (Kingma and Welling, 2014), nevertheless the basic idea is applicable to other deep generative models as well.

We suppose that physics models to be integrated can be solved analytically or numerically, and the (approximate) solution is differentiable with regard to the quantities on which the solution depends. This assumption holds in most physics models known in practice, which come in different forms such as algebraic equations, ordinary differential equations (ODEs), and partial differential equations (PDEs), with the aid of differentiable numerical integrators (see, e.g., Chen et al., 2018a) and differentiable optimizers (Amos and Kolter, 2017). Handling non-differentiable solutions and complex simulators remains an important open challenge.

2.1. Example

To demonstrate the main concepts of our approach, let us start with an example in which we have observation data of pendulums that follow the equation of motion:

$$\underbrace{d^2\theta(t)/dt^2 + \omega^2 \sin \theta(t)}_{\text{prior knowledge}} + \underbrace{\gamma d\theta(t)/dt - u(t)}_{\text{unknown}} = 0, \quad (1)$$

where θ is the pendulum’s angle, and ω , γ , and u are its frequency, damping coefficient, and external force, respectively, that may differ between different pendulums. Suppose we have prior knowledge of the first two terms only, i.e., we know that the governing equation should contain $f_P(\theta, \omega) = \ddot{\theta} + \omega^2 \sin \theta$. In order to build a generative model, we should complete f_P to learn the remaining effects of the pendulum.

We will use the available prior knowledge, f_P , by incorporating it in the decoder of a VAE. We complete f_P by equipping the decoder with an auxiliary function f_A , which we model with a neural network. The VAE’s latent variable will have two parts, z_P and z_A , respectively linked to f_P and f_A . Since z_A is a classical VAE latent variable we as-

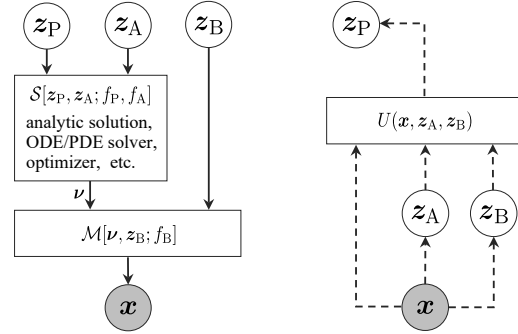


Figure 1. Physics-integrated VAEs: (left) decoding process and (right) encoding process.

sume that: $z_A \in \mathbb{R}^d$, $p(z_A) = \mathcal{N}(\mathbf{0}, \mathbf{I})$. On the other hand, we semantically ground z_P to f_P , i.e., $z_P = \omega^2 \in \mathbb{R}_{>0}$ in our example. The decoding process that will generate the observation x from the latent variables z_P, z_A , is:

$$x = \text{solve}_\theta [f_P(\theta(t), z_P) + f_A(\theta(t), z_A) = 0],$$

where $\text{solve}_\theta[f(\theta(t)) = 0]$ denotes some numerical solver of an ODE $f(\theta(t)) = 0$. Such a solver would return a sequence of solution values on an even time grid, i.e., $x = [\theta(t=0) \theta(t=\Delta t) \dots \theta(t=(\tau-1)\Delta t)]^T \in \mathbb{R}^\tau$.

2.2. General Model Description

We will now define the general model of our physics-integrated VAEs that subsumes different architectures of physics-integrated models (though most of them are not for generative modeling); details in the appendix. We give a schematic diagram of the decoding and encoding processes in Figure 1. Its latent variables z_P are directly interpretable as they are semantically grounded to the parameters of physics models f_P . The imperfections of physics models, if any, will be addressed by the learned components.

2.2.1. LATENT VARIABLES AND PRIORS

We consider three types of latent variables, z_P , z_A , and z_B . They can be in any space, but for simplicity of discussion, we suppose they are in (subsets of) the Euclidean space and set their prior distribution as multivariate normal:

$$p(z_P) = \mathcal{N}(z_P | \mathbf{m}_P, v_P^2 \mathbf{I}), \quad (2)$$

$$p(z_A) = \mathcal{N}(z_A | \mathbf{0}, \mathbf{I}), \quad (3)$$

$$p(z_B) = \mathcal{N}(z_B | \mathbf{0}, \mathbf{I}), \quad (4)$$

where \mathbf{m}_P and v_P^2 are defined in accordance with prior knowledge of physics parameters.

2.2.2. DECODER

Let x be an observation. For simplicity of discussion, suppose that the uncertainty of x can be modeled as a normal

distribution. The decoding process of physics-integrated VAEs can be concisely described as follows:

$$p_{\text{PAB}}(\mathbf{x} \mid \mathbf{z}_P, \mathbf{z}_A, \mathbf{z}_B) = \mathcal{N}(\mathbf{x} \mid f_{\text{obs}}(\boldsymbol{\mu}_{\text{PAB}}), \boldsymbol{\Sigma}_x), \quad (5)$$

$$\boldsymbol{\mu}_{\text{PAB}} = \mathcal{M}[\boldsymbol{\nu}_{\text{PA}}, \mathbf{z}_B; \{f_{B,1}, \dots, f_{B,k_B}\}], \quad (6)$$

$$\boldsymbol{\nu}_{\text{PA}} = \mathcal{S}[\mathbf{z}_P, \mathbf{z}_A; \{f_{P,1}, \dots, f_{P,k_P}\}, \{f_{A,1}, \dots, f_{A,k_A}\}], \quad (7)$$

Entities denoted by f are functions corresponding to given physics models or trainable neural networks, whereas \mathcal{M} and \mathcal{S} are functionals¹. $\boldsymbol{\Sigma}_x$ is a fixed parameter or a trainable function to estimate the variance.

\mathcal{S} is a functional corresponding to an equation solver. It takes $k_P > 0$ physics models $f_{P,1}, \dots, f_{P,k_P}$ and $k_A \geq 0$ neural networks $f_{A,1}, \dots, f_{A,k_A}$, evaluates their values given \mathbf{z}_P and \mathbf{z}_A , and solves an equation defined with $\{f_{P,i}\}$ and $\{f_{A,i}\}$. The general expression of \mathcal{S} allows various equation-solving processes to be included. The simplest case is when the equation has a closed-form solution, for which \mathcal{S} just performs function evaluations. If the equation is given as ODE or PDE, \mathcal{S} should include some numerical integrator. Some forms of equations may require \mathcal{S} to include differentiable optimizers.

\mathcal{M} is a functional that modifies the outputs of \mathcal{S} , denoted by $\boldsymbol{\nu}_{\text{PA}}$, using $k_B \geq 0$ trainable functions $f_{B,1}, \dots, f_{B,k_B}$ partly parameterized by \mathbf{z}_B . \mathcal{M} determines how these functions operate. The simplest example is $\mathcal{M} = f_B(\boldsymbol{\nu}_{\text{PA}}, \mathbf{z}_B)$. Another typical form is the so-called skip connection $\mathcal{M} = \boldsymbol{\nu}_{\text{PA}} + f_B(\boldsymbol{\nu}_{\text{PA}}, \mathbf{z}_B)$. Such a modifier \mathcal{M} is useful, for example, when the modality of equation solved in \mathcal{S} is insufficient to represent the target phenomena. Moreover, \mathcal{M} can correct the numerical errors of the solver in \mathcal{S} .

In Eq. (5), we may also consider an observation function f_{obs} , modeled also with a neural network; useful when the physics parameters and the observation data live in different spaces. In the pendulum example, the angle trajectories might not be explicitly available as data, and instead we might have access to a video recording of the pendulum.

We note that a physics model f_P can also have trainable parameters. The main distinction between the two types of functions, physics or neural nets, is whether the functional form has some physically-grounded semantics or not.

2.2.3. ENCODER

We consider the following decomposition of the posterior:

$$\begin{aligned} q_{\text{PAB}}(\mathbf{z}_P, \mathbf{z}_A, \mathbf{z}_B \mid \mathbf{x}) \\ = q(\mathbf{z}_A \mid \mathbf{x})q(\mathbf{z}_B \mid \mathbf{x})q(\mathbf{z}_P \mid \mathbf{x}, \mathbf{z}_A, \mathbf{z}_B), \end{aligned} \quad (8)$$

¹We use the functional-based notation, \mathcal{S} and \mathcal{M} , in order to describe various models in a unified form regardless of specific ways of operations of the functions, $\{f_P, i\}$, $\{f_A, i\}$, and $\{f_B, i\}$.

though other forms of dependency can be considered. Each term is parameterized as

$$q(\mathbf{z}_A \mid \mathbf{x}) = \mathcal{N}(\mathbf{z}_A \mid g_A(\mathbf{x}), \boldsymbol{\Sigma}_{z_A}), \quad (9)$$

$$q(\mathbf{z}_B \mid \mathbf{x}) = \mathcal{N}(\mathbf{z}_B \mid g_B(\mathbf{x}), \boldsymbol{\Sigma}_{z_B}), \quad (10)$$

$$\begin{aligned} q(\mathbf{z}_P \mid \mathbf{x}, \mathbf{z}_A, \mathbf{z}_B) \\ = \mathcal{N}(\mathbf{z}_P \mid g_P(U(\mathbf{x}, \mathbf{z}_A, \mathbf{z}_B)), \boldsymbol{\Sigma}_{z_P}), \end{aligned} \quad (11)$$

where g_A , g_B and g_P are so-called recognition networks. U is a neural network that will extract features useful for inferring \mathbf{z}_P , removing the effects of A- and B-part (i.e., information of \mathbf{z}_A and \mathbf{z}_B) from \mathbf{x} . We will elaborate more on U in Section 3.2.

2.3. Evidence Lower Bound

Learning and inference of VAEs are performed as usual by maximizing the lower bound of the marginal log likelihood known as evidence lower bound (ELBO). In our case,

$$\begin{aligned} \text{ELBO}(\mathbf{x}) = & \mathbb{E}_{q_{\text{PAB}}(\mathbf{z}_P, \mathbf{z}_A, \mathbf{z}_B \mid \mathbf{x})} [p_{\text{PAB}}(\mathbf{x} \mid \mathbf{z}_P, \mathbf{z}_A, \mathbf{z}_B)] \\ & + D_{\text{KL}}[q(\mathbf{z}_A \mid \mathbf{x}) \parallel p(\mathbf{z}_A)] + D_{\text{KL}}[q(\mathbf{z}_B \mid \mathbf{x}) \parallel p(\mathbf{z}_B)] \\ & + \mathbb{E}_{q(\mathbf{z}_A \mid \mathbf{x})q(\mathbf{z}_B \mid \mathbf{x})} D_{\text{KL}}[q(\mathbf{z}_P \mid \mathbf{x}, \mathbf{z}_A, \mathbf{z}_B) \parallel p(\mathbf{z}_P)]. \end{aligned} \quad (12)$$

3. Regularizing Physics-Integrated VAEs

If the trainable components of the physics-integrated VAE have sufficiently rich expression capability, as is often the case with deep neural networks, merely maximizing the ELBO in (12) provides no guarantee that the physics-based components will be used in a meaningful manner. To address this issue, we introduce semantics-preserving regularizers in the learning process.

3.1. Harnessing Neural Networks

We need to ensure that the trainable components do not dominate the behavior of the complete model and that the output of physics models is not ignored. To avoid such detrimental effects, we borrow an idea from the *posterior predictive check* (PPC), a procedure to check the validity of a statistical model (see, e.g., Gelman et al., 2013). Whereas the standard PPCs examine the discrepancy between model- and data-distribution, we want to monitor and balance the contributions of parts of a model.

We will minimize the discrepancy between the full model and its “physics-only” reduction. For the sake of argument, suppose that a given physics model is completely correct for given data. If the physics model is correctly used in the VAE, its discrepancy from the full model should be zero, since in such a case, the decoder should reduce to the physics model. Even if a physics model captures only a part of the data-generating process, the discrepancy should be

kept as small as possible, if not zero, to ensure meaningful use of the physics models in the learned VAE. We create the “physics-only” reduction of the full model by replacing its trainable functions by some simple functions. In the following, we start with a simple example and then proceed to a general definition of our PPC-based regularization using the functional-based model description.

Let us revisit the example of pendulum in Section 2.1. Recall that \mathcal{S} there is a numerical ODE solver, i.e., $\mathcal{S} = \text{solve}_\theta[f_P + f_A = 0]$. We can make a “physics-only” reduction of it by replacing the trainable part f_A by some trivial function h_A . In this case, a reasonable choice of such h_A is $h_A = 0$ because f_A appears additively in the ODE.

Now let us generalize the above idea. We refer to the VAE model defined by Eqs. (5) and (8) as the PAB-model. To construct the “physics-only” reduction of the PAB-model, we replace the trainable components, f_A and f_B , of the decoder by some trivial or less-complex functions, h_A and h_B , respectively. For simplicity let $k_P = k_A = k_B = 1$ and $f_{\text{obs}} = \text{Id}$. We show how to remove the effect of the f_A and f_B components to produce a reduced model which we call the P-model.

The decoder of the P-model is defined by modifying the PAB-model’s decoder as:

$$p_P(\mathbf{x} \mid \mathbf{z}_P, \mathbf{z}_A, \mathbf{z}_B) = \mathcal{N}(\mathbf{x} \mid \boldsymbol{\mu}_P, \boldsymbol{\Sigma}_x), \quad (13)$$

$$\boldsymbol{\mu}_P = \mathcal{M}[\boldsymbol{\nu}_P; h_B] \quad \text{and} \quad \boldsymbol{\nu}_P = \mathcal{S}[\mathbf{z}_P; f_P, h_A], \quad (14)$$

where f_A and f_B are replaced by h_A and h_B , respectively, and \mathbf{z}_A and \mathbf{z}_B are omitted from the functionals’ argument as h_A and h_B do not use them. Although \mathbf{z}_A and \mathbf{z}_B are no longer used by the P-model’s decoder p_P , we can still infer their posteriors as $q(\mathbf{z}_A \mid \mathbf{x})$ and $q(\mathbf{z}_B \mid \mathbf{x})$ in Eqs. (9) and (10). Nonetheless, as no specific realizations of \mathbf{z}_A and \mathbf{z}_B are referred to by the decoder p_P , the overall posterior q_P , which should include $q(\mathbf{z}_P \mid \mathbf{x}, \mathbf{z}_A, \mathbf{z}_B)$, should take every possibility from $q(\mathbf{z}_A \mid \mathbf{x})$ and $q(\mathbf{z}_B \mid \mathbf{x})$ into account. Consequently, we define the P-model’s encoder by marginalizing out \mathbf{z}_A and \mathbf{z}_B from q_{PAB} , that is

$$q_P(\mathbf{z}_A, \mathbf{z}_B, \mathbf{z}_P \mid \mathbf{x}) = p(\mathbf{z}_A)p(\mathbf{z}_B) \cdot \int q_{\text{PAB}}(\mathbf{z}_P, \mathbf{z}_A, \mathbf{z}_B \mid \mathbf{x}) d\mathbf{z}_A d\mathbf{z}_B. \quad (15)$$

We use the priors $p(\mathbf{z}_A)$ and $p(\mathbf{z}_B)$ to define q_P on the common support with q_{PAB} with minimal information.

We define the PA-model and the PB-model, where either of A- and B-part is reduced, analogously to the P-model. Note that, strictly speaking, only the P-model is a “physics-only” reduction, since both PA- and PB-models still have trainable neural nets f_A or f_B .

The appropriate form of the replacements, h_A and h_B , is merely a matter of model design and depends on applica-

tions, nevertheless we can give some guidelines. In most cases, the form of h should be one of the following:

- If f appears in an additive form, then usually h should be a zero-valued constant function $h = 0$;
- If f appears as a composition with another function, and its domain (modulo \mathbf{z}) and range are the same space, then h can be an identity function Id ; or
- If f appears as a composition with another function, and its domain (modulo \mathbf{z}) and range are the different spaces, then h can be a (trainable) function that has the same domain/range but a much smaller number of parameters than f , such as a (generalized) linear model and its low-rank or sparse variants.

Given the reductions (PA-, PB-, and P-models) we want to control their discrepancies from the full PAB-model. Building on PPC, we compute the discrepancy between their posterior predictive distributions. For example in the case of the PAB- and PB-models, this is:

$$D[p_{\text{PAB}}(\tilde{\mathbf{x}} \mid X) \parallel p_{\text{PB}}(\tilde{\mathbf{x}} \mid X)], \quad (16)$$

where X denotes the set of training data. While D can be any dissimilarity measure of distributions such as f -divergences and integral probability metrics, we focus on the use of the KL divergence D_{KL} .

We build a regularizer as minimization of (16) and other combinations of the reductions. However, (16) is usually computationally intractable. We instead take the following upper bound of (16) (a proof is in the appendix):

Proposition 1. *Let $p_d(\mathbf{x} \mid X)$ be the empirical distribution on the elements of X . Then, (16) can be upper bounded as*

$$D_{\text{KL}}[p_{\text{PAB}}(\tilde{\mathbf{x}} \mid X) \parallel p_{\text{PB}}(\tilde{\mathbf{x}} \mid X)] \leq \mathbb{E}_{p_d(\mathbf{x} \mid X)} \mathbb{E}_{q_{\text{PAB}}(\mathbf{z}_P, \mathbf{z}_A, \mathbf{z}_B \mid \mathbf{x})} \left[\dots D_{\text{KL}}[p_{\text{PAB}}(\tilde{\mathbf{x}} \mid \mathbf{z}_P, \mathbf{z}_A, \mathbf{z}_B) \parallel p_{\text{PB}}(\tilde{\mathbf{x}} \mid \mathbf{z}_P, \mathbf{z}_A, \mathbf{z}_B)] + D_{\text{KL}}[q_{\text{PAB}}(\mathbf{z}_P, \mathbf{z}_A, \mathbf{z}_B \mid \mathbf{x}) \parallel p(\mathbf{z}_P)p(\mathbf{z}_A)p(\mathbf{z}_B)] \right]. \quad (17)$$

Let us denote the right-hand side of (17) by $\hat{D}(\text{PAB}, \text{PB})$. We also take other combinations of the reduced models into account to compute the contributions of A-part and B-part as the sum of their marginal contributions. The upper bounds of their KL divergence can also be considered analogously to Proposition 1. Finally, we are to minimize

$$R_{\text{PPC}} = \hat{D}(\text{PAB}, \text{PB}) + \hat{D}(\text{PA}, \text{P}) + \hat{D}(\text{PAB}, \text{PA}) + \hat{D}(\text{PB}, \text{P}), \quad (18)$$

with regard to the parameters in the original model as well as the parameters of the dummy replacers h , if any.

3.2. Grounding Physics Encoder

We can utilize physics models also as a source of information by data augmentation, that is, generating additional data from them. Below we introduce additional objectives for incorporating such augmented data into learning.

We again revisit the pendulum example in Section 2.1. Since we have the (incomplete) pendulum model $f_P(\theta, \omega) = \ddot{\theta} + \omega^2 \sin \theta$ as a physics model, we can generate signals by drawing ω and solving ODE $f_P = 0$. We can then use such signals and true ω as a direct (self-)supervision of the physics-part recognition network g_P in (15). Meanwhile, the true data-generating process (i.e., (1)) has the terms of damping and external forces, which f_P misses. This is why data \mathbf{x} should be first transformed by another neural net U in (15); we expect U to perform ‘‘cleansing’’ of \mathbf{x} , which includes the effects of the unknown physics, into a signal that reflects the physics given by f_P only (i.e., no damping, no external force). We realize such U by giving another self-supervision to it.

Now let us formulate the ideas exemplified above. Let z_P^* be a sample drawn from some distribution of z_P . We artificially generate signals by

$$\nu_P^* = \mathcal{S}[z_P^*; f_P, h_A], \quad (19)$$

where h_A may or may not be the same with the replacer that appeared in (14). We want the physics-part recognition network, g_P in (15), to successfully estimate z_P^* given the corresponding ν_P^* . To this end, we provide a direct supervision to g_P as the minimization of

$$R_{g_P} = \mathbb{E}_{z_P^*} \|g_P(\nu_P^*) - z_P^*\|_2^2. \quad (20)$$

Such augmented data were used for pretraining by, e.g., Jia et al. (2019). We rather generate and use them during the main training procedure because the effects of pretraining may diminish in the main training.

While the functionality of g_P can be grounded by minimizing (20), it is only valid for the ‘‘physics-only’’ signals, which are not available unless artificially generated as above. In order to exploit the grounded functionality of g_P even for real signal \mathbf{x} , we want U in (15) to ‘‘cleanse’’ \mathbf{x} into ‘‘physics-only’’ signals like ν_P^* . Accordingly, we minimize

$$R_U = \mathbb{E}_{p_d(\mathbf{x}|X)q(z_A, z_B|\mathbf{x})} \|U(\mathbf{x}, z_A, z_B) - \mathcal{S}[g_P(U(\mathbf{x}, z_A, z_B)); f_P, h_A]\|_2^2, \quad (21)$$

where $g_P(U(\mathbf{x}, z_A, z_B))$ gives an estimation of z_P . We note that this tautological objective makes sense only if g_P is grounded by minimizing (20).

3.3. Overall Regularized Learning Objective

The overall regularized learning problem of the proposed physics-integrated VAEs is as follows:

$$\underset{f, g, h}{\text{minimize}} \quad -\mathbb{E}_{p_d(\mathbf{x}|X)} \text{ELBO} + \alpha R_{\text{PCC}} + \beta R_{g_P} + \gamma R_U,$$

where each term appears in (12), (18), (20), and (21), respectively. If we cannot specify a reasonable sampling distribution of z_P needed in (20), we do not compute (20) and (21) and set $\beta = \gamma = 0$. It may happen when the semantics of z_P are not necessarily grounded, for example, when f_P is a trainable Hamilton’s equation like in Toth et al. (2020).

4. Related Work

Physics+ML in model design Integration of physics models with machine learning models has been a subject of study for a long time and is becoming a very active area, with deep neural networks being employed in various scientific applications. Examples range from classical ones (such as Psychogios and Ungar, 1992; Rico-Martínez et al., 1994; Thompson and Kramer, 1994) to recent attempts (Young et al., 2017; Raissi, 2018; Long and She, 2018; Wan et al., 2018; Nutkiewicz et al., 2018; Ajay et al., 2018; 2019; de Bézenac et al., 2019; Zeng et al., 2019; Wang et al., 2019; Roehrl et al., 2020; Le Guen and Thome, 2020; Muralidhar et al., 2020; Belbute-Peres et al., 2020; Sengupta et al., 2020; Rackauckas et al., 2020; Li et al., 2020). Most of them focus on prediction, and the generative modeling perspective has been less investigated. Moreover, mechanisms to harness learned components have not been considered explicitly, partly because the interpretability due to physics models was not usually the main interest.

The study by Le Guen et al. (2021) is notable here, even though it is not focused on generative modeling but on dynamics learning for prediction, because they consider a mechanism to harness a learned component to preserve the utility of physics in the model. Their model can be written with our notation as $\mathbf{y} = \mathcal{S}[f_P + f_A = 0]$, where \mathcal{S} is an ODE solver, and they fit the models by minimizing $\sum \|\mathbf{y}_{\text{data}} - \mathbf{y}\|_2^2$. They suggest minimizing the function norm $\|f_A\|^2$ in the fitting procedure to harness its action. Our regularizer R_{PCC} in (18) takes quite a similar form in a special case where we have no f_B (i.e., $k_B = 0$), and f_P and f_A appear in \mathcal{S} in an additive form as above.

In generative modeling, Linial et al. (2020) developed a VAE where the latent variable follows an ODE with known functional form and unknown parameters, and the observation process is also to be learned. They also suggest grounding the semantics of the latent variable as intended by providing sparse supervision on its true value. However, it is feasible only when we have a chance to observe the latent variable

directly, for example with an increased cost. In contrast, our method does not depend on direct supervision on the latent variables, and instead use the physics models in a self-supervised manner (in Section 3.2).

Toth et al. (2020) propose Hamiltonian generative networks, where a sequence of the latent variable is governed by the Hamiltonian mechanics with a learned Hamiltonian, the encoder infers the initial condition of the sequence, and the learned decoder works as an observation function. While such models do not suppose very specific physics models but consider general mechanics, they can also be included in our modeling framework; $\mathcal{S}[f_P]$ is a symplectic integrator, and f_P is Hamilton’s equations with a learned Hamiltonian.

We also note that, apart from VAEs, the latent force models (Álvarez et al., 2009) are known as a principled method to incorporate physics models in differential equations into Gaussian processes.

Physics+ML in other approaches Another prevailing strategy is to define loss functions or regularizers based on physics knowledge (see, e.g., Stewart and Ermon, 2017; Karpatne et al., 2017b; Raissi et al., 2019; Jia et al., 2019; Yang et al., 2019; Kaltenbach and Koutsourelakis, 2020). In generative modeling, for example, Stinis et al. (2019) uses residuals from physics models as an additional feature of GAN’s discriminator.

Golany et al. (2020) regularizes the generation from GANs by forcing it close to a prescribed physics relation. These approaches are often easy to deploy, but an inherent limitation is that given physics knowledge should be complete to some extent to be utilized; e.g., a physics-based loss is not well-defined if the physics model misses important aspects of reality or has unknown parts.

Inverse problems with ML It is not surprising that the ideas of inverse problems are in line with the auto-encoding variational Bayes; in inverse problems, the forward process (i.e., a decoder) is known and a corresponding backward process (i.e., an encoder) is to be estimated. For example, Tait and Damoulas (2020) propose to solve inverse problem using a VAE in which the decoder has a structure based on the finite element method for PDEs. Aragon-Calvo and Carvajal (2020) replace VAE’s decoder by a light distribution model of galaxies for inferring physically-meaningful parameters from galaxy images. The framework we proposed can also be applied to such problems.

Broader perspectives Integration of physics models into data-driven models in general is also related to broader range of topics such as causality in machine learning, data assimilation, and model discrepancy. In addition, efficient integration of physics and data-driven models can be facilitated with techniques developed in areas such as PDE-constrained optimization and likelihood-free inference.

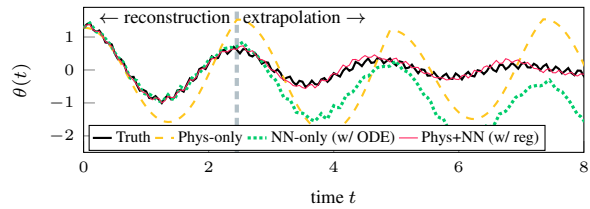


Figure 2. Reconstruction and extrapolation of a test sample of the pendulum data. The signals in range $0 \leq t < 2.5$ are the result of reconstruction, whereas in $t \geq 2.5$ they are extrapolation.

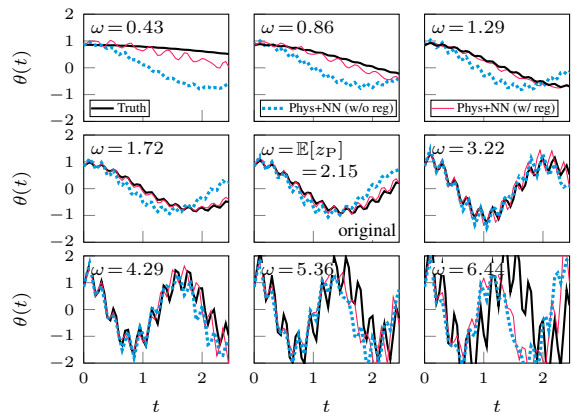


Figure 3. Counterfactual generation for the pendulum data. The center panel shows the original reconstruction, and the rest is the generation with z_P (i.e., ω) being changed while $z_{A,B}$ being fixed.

5. Experiments

We performed experiments on two synthetic datasets and two real-world datasets, for which we prepared instances of physics-integrated VAEs. We show each particular architecture of physics-integrated VAEs and the corresponding results. Some details are deferred to the appendix.

5.1. Forced Damped Pendulum

Dataset We generated data from the ODE of a pendulum (1) with $u(t) = A\omega^2 \cos(2\pi\phi t)$. Each data-point x is a sequence $x = [\theta_1 \dots \theta_\tau] \in \mathbb{R}^\tau$, where θ_j is the value of a solution $\theta(t_j)$ at $t_j = (j-1)\Delta t$. We randomly drew a sample of the initial condition θ_1 (with $\dot{\theta}_1 = 0$ fixed) and the values of ω , γ , A , and ϕ for each sequence. We generated 2,500 sequences of length $\tau = 50$ with $\Delta t = 0.05$ and separated them into a training, validation, and test sets with 1,000, 500, and 1,000 sequences, respectively. We did not use a nontrivial observation mechanism f_{obs} , so that we can directly examine what is generated by a physics-integrated VAE. Capability of learning such an observation function has already been investigated (e.g., Toth et al., 2020).

Decoder We set $k_P = k_A = k_B = 1$. We set f_P as in the example in Section 2.1, i.e., $f_P(\theta, z_P) = \ddot{\theta} + z_P^2 \sin(\theta)$,

where $z_P \in \mathbb{R}$ should work as ω . We augmented it by $f_A(\theta, z_A)$ additively, where f_A is a multi-layer perceptron (MLP) with two hidden layers, and $z_A \in \mathbb{R}$. Hence, $\mathcal{S}[z_P, z_A; f_P, f_A]$ is a numerical ODE solver with the Euler update scheme that returns the solution of ODE $f_P(\theta, z_P) + f_A(\theta, z_A) = 0$ at even time grid from $t = 0$ to $t = (\tau - 1)\Delta t$. Another MLP f_B is for correcting \mathcal{S} 's output by $\mathcal{M}[z_B; f_B] = f_B([\mathcal{S}[\cdot]^T z_B^T]^T)$. We set $f_{\text{obs}} = \text{Id}$.

Encoder g_A, g_B, U , and g_P are all modeled with MLPs. We used the initial element of each sequence \mathbf{x} as an estimation of the initial condition θ_1 .

Setting We compare the proposed physics-integrated VAE (called the Phys+NN model hereafter) with the following:

1. Physics-only model, where f_A and f_B are replaced with zero and identity functions, respectively (i.e., P-model);
2. NN-only VAE model *without* ODE solver in the decoder, where $f_P = f_A = 0$ (i.e., something like B-model);
3. NN-only VAE model *with* ODE solver, where $f_P = 0$ but f_A is still alive (i.e., AB-model); and
4. Phys+NN VAE model learned *without* proposed regularizers (i.e., PAB-model trained with $\alpha = \beta = \gamma = 0$; similar to Linial et al. (2020)).

We set $\dim z_A = 1$ and $\dim z_B = 2$ in the full PAB-model. For the baseline models, we increased $\dim z_A$ and/or $\dim z_B$ accordingly to compensate the lack of z_P (or z_A); for example, we set $\dim z_A = \dim z_B = 2$ for the NN-only with ODE, i.e., AB-model. Consequently, every model has the same dimensionality of z 's in total.

Results We show the reconstruction error and the inference error of physics parameter ω on the test set in Table 1. The errors are reported in mean absolute errors (MAEs). The inference error of ω is evaluated by $|\mathbb{E}[z_P] - \omega_{\text{true}}|$. Table 1 clearly shows that only the physics-integrated VAE with the proposed regularizers achieve small values in both reconstruction error and inference error.

In Figure 2, we show an example of reconstruction with extrapolation. Recall that the training data is sequences of range $0 \leq t < 2.5$ only; so $t \geq 2.5$ is extrapolation. We can observe that while the NN-only model cannot extrapolate, the Phys+NN VAE can reconstruct well as well as extrapolate correctly. We note that all the models, including Phys+NN, are *not* directly informed of the damping effect and the external force; they were to be learned from data.

In Figure 3, we show an example of generating signals from the learned model while manipulating z_P ; recall that z_P is expected to work as pendulum's frequency ω in (1). We took a test sample with $\mathbb{E}[z_P] \approx 2.15$. For this sample, the center panel of Figure 3 shows the original data and the reconstruction by the Phys+NN model. We then generated signals with different values of z_P (i.e., ω), keeping the values of

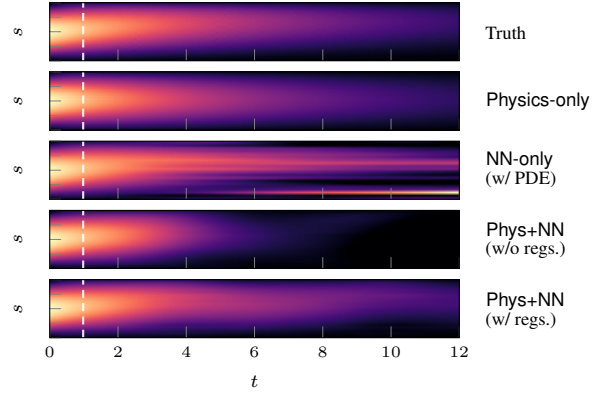


Figure 4. Reconstruction and extrapolation of a test sample of the convection-diffusion data. Range $0 \leq t < 1$ is reconstruction, whereas $t \geq 1$ is extrapolation; the dashed line is the border.

z_A and z_B to be the original posterior mean. The results are shown in the remaining panels of Figure 3. We can see that the generated signals match well with the signals from the true process, while some deviation is observed when z_P is far from the original value. Note that the training data was generated with ω from $[0.785, 3.14]$; the Phys+NN, if properly regularized, can generate signals beyond that range (i.e., extrapolation in parameter).

5.2. Advection-Diffusion System

Dataset We generated data from advection-diffusion PDE:

$$\partial T / \partial t - a \cdot \partial^2 T / \partial s^2 + b \cdot \partial T / \partial s = 0, \quad (22)$$

where s is the 1-D spatial dimension. We approximated the solution $T(s, t)$ on the 12-point even grid from $s = 0$ to $s = s_{\text{max}}$, so each data-point \mathbf{x} is a sequence of 12-dim vectors, i.e., $\mathbf{x} = [\mathbf{T}_1 \cdots \mathbf{T}_\tau] \in \mathbb{R}^{12 \times \tau}$, where $\mathbf{T}_j = [T(0, (j-1)\Delta t) \cdots T(s_{\text{max}}, (j-1)\Delta t)]^T$. We set the boundary condition as $T(0, t) = T(s_{\text{max}}, t) = 0$ and the initial condition as $T(s, 0) = c \sin(\pi s / s_{\text{max}})$. We randomly drew the values of a , b , and c for each data-point. We generated 2,500 sequences with $\tau = 50$ and $\Delta t = 0.02$ and separated them into a training, validation, and test sets with 1,000, 500, and 1,000 sequences, respectively.

Decoder We set $k_P = k_A = 1$ whereas $k_B = 0$. We used a part of (22) as f_P , i.e., $f_P(T, z_P) = \partial T / \partial t - z_P \partial^2 T / \partial s^2$, where $z_P \in \mathbb{R}$ should work as a . We augmented it by $f_A(y, z_A)$ additively, where f_A is an MLP with two hidden layers, and $z_A \in \mathbb{R}^4$. Hence, $\mathcal{S}[z_P, z_A; f_P, f_A]$ is a numerical solver with the explicit finite different scheme that returns the solution of PDE $f_P(y, z_P) + f_A(y, z_A) = 0$ at even time grid from $t = 0$ to $t = (\tau - 1)\Delta t$.

Encoder g_A, U , and g_P are all modeled with MLPs. We used the initial snapshot of each sequence \mathbf{x} as an estimation of the initial condition \mathbf{T}_1 .

Table 1. Performances on test set of the pendulum data. Averages (and SDs) over 20 random trials are reported.

| | MAE of reconstruction | | MAE of inferred ω | |
|--------------------|-----------------------|------------------------|--------------------------|------------------------|
| Physics-only | 1.55 | (7.1×10^{-4}) | 0.232 | (5.9×10^{-3}) |
| NN-only, w/o ODE | 0.438 | (2.9×10^{-2}) | – | – |
| NN-only, w/ ODE | 0.439 | (2.3×10^{-2}) | – | – |
| Phys+NN, w/o regs. | 0.370 | (4.3×10^{-2}) | 1.04 | (2.2×10^{-1}) |
| Phys+NN, w/ regs. | 0.363 | (4.8×10^{-2}) | 0.229 | (3.8×10^{-2}) |

Table 2. Performances on test set of the locomotion data. Averages (and SDs) over 20 random trials are reported.

| | MAE of reconstruction | |
|--------------------|-----------------------|------------------------|
| Physics-only | 0.726 | (1.0×10^{-2}) |
| NN-only, w/ ODE | 0.276 | (1.5×10^{-2}) |
| Phys+NN, w/o regs. | 0.273 | (9.0×10^{-3}) |
| Phys+NN, w/ regs. | 0.259 | (9.0×10^{-3}) |



Figure 5. (left) Subset of the galaxy image data. (right three) Random generation from the NN-only model and the Phys+NN models.

Setting We set $\dim z_A = 4$ for the full PA-model (recall that PA is the full model as $k_B = 0$). The remaining setting is similar to the ones in Section 5.1.

Results The physics-integrated VAE with the proposed regularizers achieved good performance both in reconstruction and a 's inference (full results are in the appendix).

In Figure 4, we show an example of reconstruction with extrapolation. As the training data only comprise sequences of range $0 \leq t < 1$, the remaining range $t \geq 1$ is extrapolation. The extrapolation by the Physics-only does not consider advection, and the NN-only model shows unnatural artifacts. In contrast, the regularized Phys+NN model (bottom panel of Figure 4) successfully extrapolates beyond the training data range of time. Meanwhile, the diffusion coefficient a is wrongly inferred by Phys+NN without the proposed regularization (second from the bottom), which results in the inaccurate extrapolation.

5.3. Galaxy Images

Dataset We used images of galaxy from a part of the Galaxy10 dataset². We selected the 589 images of the ‘‘Disk, Edge-on, No Bulge’’ class and separated them into training, validation, and test sets with 400, 100, and 89 images, respectively. Each image is of size 69×69 with three channels. A subset of the test set is shown in Figure 5.2. In training, we performed classical data augmentation with random rotation and increased the size of the training set by 20 times.

Decoder We set $k_P = k_B = 1$, whereas $k_A = 0$. The physics model $f_P: \mathbb{R}^4 \rightarrow \mathbb{R}^{69 \times 69}$ is an exponential profile of the light distribution of galaxies whose input is $z_P =$

²The original images are from the Sloan Digital Sky Survey www.sdss.org, and the labels are from the Galaxy Zoo project www.galaxyzoo.org. The dataset is available a part of the astroNN package (Leung and Bovy, 2018)

$[I_0 \ A \ B \ \theta]^T \in \mathbb{R}_{>0}^4$. \mathcal{S} is just a function evaluation, i.e., $\mathcal{S}[z_P; f_P] = f_P(z_P)$. Let $[f_P]_{i,j}$ denote the (i, j) -element of the output of f_P . Then, for $1 \leq i, j \leq 69$,

$$[f_P]_{i,j} = I_0 \exp(-r_{i,j}), \quad \text{where} \quad (23)$$

$$r_{i,j}^2 = (X_j \cos \theta - Y_i \sin \theta)^2 / A^2 + (X_j \sin \theta + Y_i \cos \theta)^2 / B^2,$$

where (X_j, Y_i) is the coordinate on the 69×69 even grid on $[-1, 1] \times [-1, 1]$. This model was used in a similar problem of Aragon-Calvo and Carvajal (2020), where they only handle artificial images. As we deal with real images, we modify the output of f_P using a U-Net-like neural network $f_B: \mathbb{R}^{69 \times 69} \times \mathbb{R}^{\dim z_B} \rightarrow \mathbb{R}^{69 \times 69 \times 3}$.

Encoder Given an image $x \in \mathbb{R}^{69 \times 69 \times 3}$, we first extract features using a convolutional neural network as in Aragon-Calvo and Carvajal (2020). We then flatten the extracted features and give them to g_P and g_B , both of which are an MLP with two hidden layers.

Setting We examined the Phys+NN model with $\dim z_B = 2$ (because $\dim z_P = 4$) and the NN-only model with $\dim z_B = 6$. We did not use R_{g_P} , i.e., set $\beta = 0$.

Results In Figure 5, we show the images generated randomly from the learned models. Whereas the NN-only model tends to generate many non-realistic images, the Phys+NN model with the proposed regularization consistently generates galaxy-like images. The generation without R_{PPC} (i.e., setting $\alpha = 0$) is slightly better than NN-only but still looks spurious.

5.4. Human Locomotion

Dataset We used a part of the dataset provided by Lencioni et al. (2019), which contains measurements of walks of 50 subjects at different speeds. We extracted the angles of hip, knee, and ankle in the sagittal plane. Data

originally comprise sequences of each stride normalized to be 100 steps, so each data-point \mathbf{x} is a sequence $\mathbf{x} = [\theta_1 \dots \theta_{100}] \in \mathbb{R}^{3 \times 100}$, where $\theta_j = [\theta_{\text{hip},j} \ \theta_{\text{knee},j} \ \theta_{\text{ankle},j}]^\top$. We used different 400, 100, and 344 sequences as training, validation, and test sets, respectively.

Decoder We set $k_P = k_B = 1$, whereas $k_A = 0$. Modeling of bipedal locomotion is a long-standing problem of biomechanics (see, e.g., Robertson et al., 2014). We did not choose a specific model but let f_P be a trainable Hamilton’s equation as in Toth et al. (2020); Greydanus et al. (2019):

$$f_P \left([\mathbf{p}^\top \ \mathbf{q}^\top]^\top \right) = \left[-\frac{\partial \mathcal{H}}{\partial \mathbf{q}}^\top \ \frac{\partial \mathcal{H}}{\partial \mathbf{p}}^\top \right]^\top, \quad (24)$$

where $\mathbf{p} \in \mathbb{R}^{d_y}$ is a generalized position, $\mathbf{q} \in \mathbb{R}^{d_y}$ is a generalized momentum, and $\mathcal{H}: \mathbb{R}^{d_y} \times \mathbb{R}^{d_y} \rightarrow \mathbb{R}$ is a Hamiltonian. Hence, \mathcal{S} is a solver of ODE $f_P = 0$. We let $d_y = 3$ and modeled \mathcal{H} with an MLP with two hidden layers. The trajectory of \mathbf{p} is then transformed by f_B .

Encoder We modeled the recognition network g_B with an MLP with four hidden layers. g_P is another MLP and infers the initial condition of \mathbf{p} and \mathbf{q} .

Setting We set $\dim \mathbf{z}_B = 15$ for the full PB-model. The remaining setting is similar to the ones in Section 5.1.

Results We show the test reconstruction errors in Table 2, wherein the regularized Phys+NN model achieves the best performance. The difference of the behavior of the learned models is more comprehensible when examined visually; Figure 6 compares the reconstructions by two versions of the Phys+NN model, trained without or with the proposed regularizers. The dashed lines show the intermediate of reconstruction, i.e., the output of Hamiltonian mechanics $\mathcal{S}[f_P]$, and the red solid lines show the final reconstruction, i.e., the output of $f_B(\mathcal{S}[f_P])$. Without regularization, the physics-based part $\mathcal{S}[f_P]$ returns meaningless signal, and f_B bears the most effort of reconstruction. On the other hand, with the proposed regularization, $\mathcal{S}[f_P]$ well match the data, and f_B modifies it only slightly.

6. Conclusion

Physics-integrated VAEs by construction attain partial interpretability as some of the latent variables are semantically grounded to the physics models, and thus we can generate signals in a controlled manner. Moreover, they have extrapolation capability due to the physics models. In this work, we provided a general description of physics-integrated VAEs, and proposed a regularized learning objective for ensuring a proper functionality of the integrated physics models. We also empirically validated the aforementioned unique capability of physics-integrated VAEs.

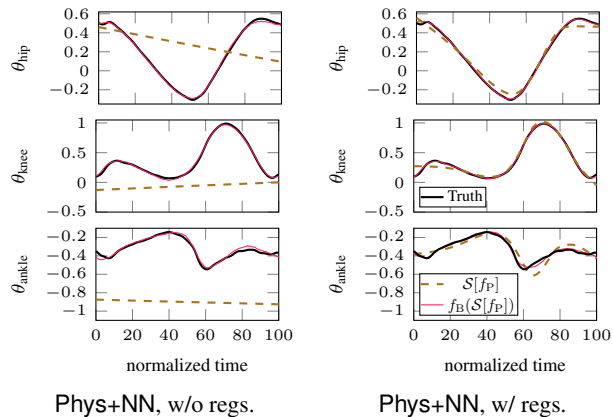


Figure 6. Example of reconstruction on the locomotion data with the Phys+NN model. $\mathcal{S}[f_P]$ is an intermediate value of the decoder, and $f_B(\mathcal{S}[f_P])$ is the final output.

Acknowledgements

This work was supported by the Innosuisse project *Industrial artificial intelligence for intelligent machines and manufacturing digitalization* (39453.1 IP-ICT) and the Swiss National Science Foundation Sinergia project *Modeling pathological gait resulting from motor impairments* (CR-SII5_177179).

References

- A. Ajay, J. Wu, N. Fazeli, M. Bauza, L. P. Kaelbling, J. B. Tenenbaum, and A. Rodriguez. Augmenting physical simulators with stochastic neural networks: Case study of planar pushing and bouncing. In *Proceedings of the 2018 IEEE/RSJ International Conference on Intelligent Robots and Systems*, pages 3066–3073, 2018.
- A. Ajay, M. Bauza, J. Wu, N. Fazeli, J. B. Tenenbaum, A. Rodriguez, and L. P. Kaelbling. Combining physical simulators and object-based networks for control. In *Proceedings of the 2019 IEEE International Conference on Robotics and Automation*, pages 3217–3223, 2019.
- M. Álvarez, D. Luengo, and N. D. Lawrence. Latent force models. In *Proceedings of the 12th International Conference on Artificial Intelligence and Statistics*, pages 9–16, 2009.
- B. Amos and J. Z. Kolter. OptNet: Differentiable optimization as a layer in neural networks. In *Proceedings of the 34th International Conference on Machine Learning*, pages 136–145, 2017.
- M. A. Aragon-Calvo and J. C. Carvajal. Self-supervised learning with physics-aware neural networks – I. Galaxy model fitting. *Monthly Notices of the Royal Astronomical Society*, 498(3):3713–3719, 2020.

- S. Ö. Arik, C.-L. Li, J. Yoon, R. Sinha, A. Epshteyn, L. T. Le, V. Menon, S. Singh, L. Zhang, N. Yoder, M. Nikoltchev, Y. Sonthalia, H. Nakhost, E. Kanal, and T. Pfister. Interpretable sequence learning for COVID-19 forecasting. arXiv:2008.00646, 2020.
- Y. Ba, G. Zhao, and A. Kadambi. Blending diverse physical priors with neural networks. arXiv:1910.00201, 2019.
- A. Behjat, C. Zeng, R. Rai, I. Matei, D. Doermann, and S. Chowdhury. A physics-aware learning architecture with input transfer networks for predictive modeling. *Applied Soft Computing*, 96:106665, 2020.
- F. d. A. Belbute-Peres, T. D. Economon, and J. Z. Kolter. Combining differentiable PDE solvers and graph neural networks for fluid flow prediction. In *Proceedings of the 37th International Conference on Machine Learning*, pages 2402–2411, 2020.
- G. Camps-Valls, D. H. Svendsen, J. Cortés-Andrés, Á. Moreno-Martínez, A. Pérez-Suay, J. Adsuaara, I. Martín, M. Piles, J. Muñoz-Marí, and L. Martino. Living in the physics and machine learning interplay for earth observation. arXiv:2010.09031, 2020.
- T. Q. Chen, Y. Rubanova, J. Bettencourt, and D. K. Duvenaud. Neural ordinary differential equations. In *Advances in Neural Information Processing Systems 31*, pages 6572–6583, 2018a.
- X. Chen, X. Xu, X. Liu, S. Pan, J. He, H. Y. Noh, L. Zhang, and P. Zhang. PGA: Physics guided and adaptive approach for mobile fine-grained air pollution estimation. In *Proceedings of the 2018 ACM International Joint Conference on Pervasive and Ubiquitous Computing and Wearable Computers*, pages 1321–1330, 2018b.
- M. Cranmer, S. Greydanus, S. Hoyer, P. Battaglia, D. Spergel, and S. Ho. Lagrangian neural networks. arXiv:2003.04630, 2020.
- E. de Bézenac, A. Pajot, and P. Gallinari. Deep learning for physical processes: Incorporating prior scientific knowledge. *Journal of Statistical Mechanics: Theory and Experiment*, 2019(12):124009, 2019.
- W. De Groote, E. Kikken, E. Hostens, S. Van Hoecke, and G. Crevecoeur. Neural network augmented physics models for systems with partially unknown dynamics: Application to slider-crank mechanism. arXiv:1910.12212, 2019.
- M. Déchelle, J. Donà, K. Plessis-Fraissard, P. Gallinari, and M. Levy. Bridging dynamical models and deep networks to solve forward and inverse problems. NeurIPS workshop on Interpretable Inductive Biases and Physically Structured Learning, 2020.
- A. Gelman, J. B. Carlin, H. S. Stern, D. B. Dunson, A. Vehtar, and D. B. Rubin. *Bayesian Data Analysis*. Chapman and Hall/CRC, 3rd edition, 2013.
- T. Golany, D. Freedman, and K. Radinsky. SimGANs: Simulator-based generative adversarial networks for ECG synthesis to improve deep ECG classification. In *Proceedings of the 37th International Conference on Machine Learning*, pages 3597–3606, 2020.
- F. Golemo, P.-Y. Oudeyer, A. A. Taïga, and A. Courville. Sim-to-real transfer with neural-augmented robot simulation. In *Proceedings of the 2nd Conference on Robot Learning*, pages 817–828, 2018.
- S. Greydanus, M. Dzamba, and J. Yosinski. Hamiltonian neural networks. In *Advances in Neural Information Processing Systems 32*, pages 15379–15389, 2019.
- E. Heiden, D. Millard, E. Coumans, Y. Sheng, and G. S. Sukhatme. NeuralSim: Augmenting differentiable simulators with neural networks. arXiv:2011.04217, 2020.
- X. Jia, J. Willard, A. Karpatne, J. Read, J. Zwart, M. Steinbach, and V. Kumar. Physics guided RNNs for modeling dynamical systems: A case study in simulating lake temperature profiles. In *Proceedings of the 2019 SIAM International Conference on Data Mining*, pages 558–566, 2019.
- Y. Jiang, J. Sun, and C. K. Liu. Data-augmented contact model for rigid body simulation. arXiv:1803.04019, 2018.
- Y. Jiang, T. Zhang, D. Ho, Y. Bai, C. K. Liu, S. Levine, and J. Tan. SimGAN: Hybrid simulator identification for domain adaptation via adversarial reinforcement learning. arXiv:2101.06005, 2021.
- S. Kaltenbach and P.-S. Koutsourelakis. Incorporating physical constraints in a deep probabilistic machine learning framework for coarse-graining dynamical systems. *Journal of Computational Physics*, 419:109673, 2020.
- S. Kaltenbach and P.-S. Koutsourelakis. Physics-aware, probabilistic model order reduction with guaranteed stability. In *Proceedings of the 9th International Conference on Learning Representations*, 2021.
- A. Karpatne, G. Atluri, J. Faghmous, M. Steinbach, A. Banerjee, A. Ganguly, S. Shekhar, N. Samatova, and V. Kumar. Theory-guided data science: A new paradigm for scientific discovery from data. *IEEE Transactions on Knowledge and Data Engineering*, 29(10):2318–2331, 2017a.
- A. Karpatne, W. Watkins, J. Read, and V. Kumar. Physics-guided neural networks (PGNN): An application in lake temperature modeling. arXiv:1710.11431, 2017b.

- D. P. Kingma and M. Welling. Auto-encoding variational Bayes. In *Proceedings of the 2nd International Conference on Learning Representations*, 2014.
- F. Lanusse, P. Melchior, and F. Moolekamp. Hybrid physical-deep learning model for astronomical inverse problems. arXiv:1912.03980, 2019.
- V. Le Guen and N. Thome. Disentangling physical dynamics from unknown factors for unsupervised video prediction. In *Proceedings of the 2020 IEEE/CVF Conference on Computer Vision and Pattern Recognition*, pages 11471–11481, 2020.
- V. Le Guen, Y. Yin, J. Dona, I. Ayed, E. de Bézenac, N. Thome, and P. Gallinari. Augmenting physical models with deep networks for complex dynamics forecasting. In *Proceedings of the 9th International Conference on Learning Representations*, 2021.
- T. Lencioni, I. Carpinella, M. Rabuffetti, A. Marzegan, and M. Ferrarin. Human kinematic, kinetic and EMG data during different walking and stair ascending and descending tasks. *Scientific Data*, 6(1):309, 2019.
- H. W. Leung and J. Bovy. Deep learning of multi-element abundances from high-resolution spectroscopic data. *Monthly Notices of the Royal Astronomical Society*, 483(3):3255–3277, 2018.
- L. Li, S. Hoyer, R. Pederson, R. Sun, E. D. Cubuk, P. Riley, and K. Burke. Kohn-Sham equations as regularizer: Building prior knowledge into machine-learned physics. *Physical Review Letters*, 126(3):036401, 2020.
- O. Linial, D. Eytan, and U. Shalit. Generative ODE modeling with known unknowns. arXiv:2003.10775, 2020.
- Y. Long and X. She. HybridNet: Integrating model-based and data-driven learning to predict evolution of dynamical systems. In *Proceedings of the 2nd Conference on Robot Learning*, pages 551–560, 2018.
- M. Lutter, C. Ritter, and J. Peters. Deep Lagrangian networks: Using physics as model prior for deep learning. In *Proceedings of the 7th International Conference on Learning Representations*, 2019.
- I. Matei, J. de Kleer, C. Somarakis, R. Rai, and J. S. Baras. Interpretable machine learning models: A physics-based view. arXiv:2003.10025, 2020.
- V. Mehta, I. Char, W. Neiswanger, Y. Chung, A. O. Nelson, M. D. Boyer, E. Kolemen, and J. Schneider. Neural dynamical systems: Balancing structure and flexibility in physical prediction. arXiv:2006.12682, 2020.
- A. T. Mohan, N. Lubbers, D. Livescu, and M. Chertkov. Embedding hard physical constraints in neural network coarse-graining of 3D turbulence. arXiv:2002.00021, 2020.
- N. Muralidhar, J. Bu, Z. Cao, L. He, N. Ramakrishnan, D. Tafti, and A. Karpatne. PhyNet: Physics guided neural networks for particle drag force prediction in assembly. In *Proceedings of the 2020 SIAM International Conference on Data Mining*, pages 559–567, 2020.
- A. Nutkiewicz, Z. Yang, and R. K. Jain. Data-driven Urban Energy Simulation (DUE-S): A framework for integrating engineering simulation and machine learning methods in a multi-scale urban energy modeling workflow. *Applied Energy*, 225:1176–1189, 2018.
- S. Pawar, O. San, B. Aksoylu, A. Rasheed, and T. Kvamsdal. Physics guided machine learning using simplified theories. arXiv:2012.13343, 2020.
- D. C. Psychogios and L. H. Ungar. A hybrid neural network-first principles approach to process modeling. *AIChE Journal*, 38(10):1499–1511, 1992.
- C. Rackauckas, Y. Ma, J. Martensen, C. Warner, K. Zubov, R. Supekar, D. Skinner, A. Ramadhan, and A. Edelman. Universal differential equations for scientific machine learning. arXiv:2001.04385, 2020.
- M. Raissi. Deep hidden physics models: Deep learning of nonlinear partial differential equations. *Journal of Machine Learning Research*, 19(25):1–24, 2018.
- M. Raissi, P. Perdikaris, and G. E. Karniadakis. Physics-informed neural networks: A deep learning framework for solving forward and inverse problems involving nonlinear partial differential equations. *Journal of Computational Physics*, 378:686–707, 2019.
- R. Reinhart, Z. Shareef, and J. Steil. Hybrid analytical and data-driven modeling for feed-forward robot control. *Sensors*, 17(2):311, 2017.
- H. Ren, R. Stewart, J. Song, V. Kuleshov, and S. Ermon. Learning with weak supervision from physics and data-driven constraints. *AI Magazine*, 39(1):27–38, 2018.
- R. Rico-Martínez, J. S. Anderson, and I. G. Kevrekidis. Continuous-time nonlinear signal processing: A neural network based approach for gray box identification. In *Proceedings of the IEEE Workshop on Neural Networks for Signal Processing*, pages 596–605, 1994.
- D. G. E. Robertson, G. E. Caldwell, J. Hamill, G. Kamen, and S. N. Whittlesey. *Research Methods in Biomechanics. Human Kinetics*, 2nd edition, 2014.

- M. A. Roehrl, T. A. Runkler, V. Brandtstetter, M. Tokic, and S. Obermayer. Modeling system dynamics with physics-informed neural networks based on Lagrangian mechanics. *arXiv:2005.14617*, 2020.
- S. Saemundsson, A. Terenin, K. Hofmann, and M. Deisenroth. Variational integrator networks for physically structured embeddings. In *Proceedings of the 23rd International Conference on Artificial Intelligence and Statistics*, pages 3078–3087, 2020.
- B. Schölkopf, F. Locatello, S. Bauer, N. R. Ke, N. Kalchbrenner, A. Goyal, and Y. Bengio. Towards causal representation learning. *arXiv:2102.11107*, 2021.
- U. Sengupta, M. Amos, J. S. Hosking, C. E. Rasmussen, M. Juniper, and P. J. Young. Ensembling geophysical models with Bayesian neural networks. In *Advances in Neural Information Processing Systems 33*, 2020.
- N. Shlezinger, J. Whang, Y. C. Eldar, and A. G. Dimakis. Model-based deep learning. *arXiv:2012.08405*, 2020.
- S. K. Singh, R. Yang, A. Behjat, R. Rai, S. Chowdhury, and I. Matei. PI-LSTM: Physics-infused long short-term memory network. In *Proceedings of the 18th IEEE International Conference on Machine Learning and Applications*, pages 34–41, 2019.
- R. Stewart and S. Ermon. Label-free supervision of neural networks with physics and domain knowledge. In *Proceedings of the 31st AAAI Conference on Artificial Intelligence*, pages 2576–2582, 2017.
- P. Stinis, T. Hagge, A. M. Tartakovsky, and E. Yeung. Enforcing constraints for interpolation and extrapolation in generative adversarial networks. *Journal of Computational Physics*, 397:108844, 2019.
- D. J. Tait and T. Damoulas. Variational autoencoding of PDE inverse problems. *arXiv:2006.15641*, 2020.
- M. L. Thompson and M. A. Kramer. Modeling chemical processes using prior knowledge and neural networks. *AIChE Journal*, 40(8):1328–1340, 1994.
- P. Toth, D. J. Rezende, A. Jaegle, S. Racanière, A. Botev, and I. Higgins. Hamiltonian generative networks. In *Proceedings of the 8th International Conference on Learning Representations*, 2020.
- F. A. Viana, R. G. Nascimento, A. Dourado, and Y. A. Yucesan. Estimating model inadequacy in ordinary differential equations with physics-informed neural networks. *Computers & Structures*, 245:106458, 2021.
- L. von Rueden, S. Mayer, K. Beckh, B. Georgiev, S. Giesselbach, R. Heese, B. Kirsch, J. Pfommer, A. Pick, R. Ramamurthy, M. Walczak, J. Garcke, C. Bauckhage, and J. Schuecker. Informed machine learning – A taxonomy and survey of integrating knowledge into learning systems. *arXiv:1903.12394v2*, 2020.
- Z. Y. Wan, P. Vlachas, P. Koumoutsakos, and T. Sapsis. Data-assisted reduced-order modeling of extreme events in complex dynamical systems. *PLOS ONE*, 13(5):e0197704, 2018.
- Q. Wang, F. Li, Y. Tang, and Y. Xu. Integrating model-driven and data-driven methods for power system frequency stability assessment and control. *IEEE Transactions on Power Systems*, 34(6):4557–4568, 2019.
- J. Willard, X. Jia, S. Xu, M. Steinbach, and V. Kumar. Integrating physics-based modeling with machine learning: A survey. *arXiv:2003.04919*, 2020.
- L. Yang, X. Meng, and G. E. Karniadakis. B-PINNs: Bayesian physics-informed neural networks for forward and inverse PDE problems with noisy data. *Journal of Computational Physics*, 425:109913, 2021.
- Y. Yang and P. Perdikaris. Physics-informed deep generative models. *arXiv:1812.03511*, 2018.
- Z. Yang, J.-L. Wu, and H. Xiao. Enforcing deterministic constraints on generative adversarial networks for emulating physical systems. *arXiv:1911.06671*, 2019.
- Ç. Yıldız, M. Heinonen, and H. Lähdesmäki. ODE2VAE: Deep generative second order ODEs with Bayesian neural networks. In *Advances in Neural Information Processing Systems 32*, pages 13412–13421, 2019.
- C.-C. Young, W.-C. Liu, and M.-C. Wu. A physically based and machine learning hybrid approach for accurate rainfall-runoff modeling during extreme typhoon events. *Applied Soft Computing*, 53:205–216, 2017.
- A. Zeng, S. Song, J. Lee, A. Rodriguez, and T. Funkhouser. TossingBot: Learning to throw arbitrary objects with residual physics. In *Proceedings of Robotics: Science and Systems*, 2019.
- Z. Zhang, R. Rai, S. Chowdhury, and D. Doermann. MID-PhyNet: Memorized infusion of decomposed physics in neural networks to model dynamic systems. *Neurocomputing*, 428:116–129, 2021.
- S. Zhao, J. Song, and S. Ermon. InfoVAE: Balancing learning and inference in variational autoencoders. In *Proceedings of the 33rd AAAI Conference on Artificial Intelligence*, pages 5885–5892, 2019.

A. Proof of Proposition 1

Proof. Let $p_1(x, y)$ and $p_2(x, y)$ be two joint distributions on random variables x and y , and $p_1(x)$ and $p_2(x)$ be the corresponding marginals. Then, from $p(x)p(y | x) = p(x, y)$ and the nonnegativity of the KL divergence,

$$\begin{aligned} D_{\text{KL}}[p_1(x) \parallel p_2(x)] &= \int p_1(x) \log \frac{p_1(x)}{p_2(x)} dx \\ &= \int \frac{p_1(x, y)}{p_1(y | x)} \log \frac{p_1(x, y)p_2(x | y)}{p_1(y | x)p_2(x, y)} dx dy \\ &= D_{\text{KL}}[p_1(x, y) \parallel p_2(x, y)] \\ &\quad - D_{\text{KL}}[p_1(y | x) \parallel p_2(y | x)] \\ &\leq D_{\text{KL}}[p_1(x, y) \parallel p_2(x, y)]. \end{aligned} \quad (25)$$

Let us denote the set of latent variables z_P , z_A , and z_B collectively by z for simplicity. We apply (25) to the KL divergence in between the posterior predictive distributions of the PAB- and p_{PB} models as follows:

$$\begin{aligned} D_{\text{KL}}[p_{\text{PAB}}(\tilde{x} | X) \parallel p_{\text{PB}}(\tilde{x} | X)] &\leq D_{\text{KL}}[p_{\text{PAB}}(\tilde{x}, z, \mathbf{x} | X) \parallel p_{\text{PB}}(\tilde{x}, z, \mathbf{x} | X)] \\ &= D_{\text{KL}}[p_{\text{PAB}}(\tilde{x} | z)q_{\text{PAB}}(z | \mathbf{x})p_d(\mathbf{x} | X) \\ &\quad \parallel p_{\text{PB}}(\tilde{x} | z)q_{\text{PB}}(z | \mathbf{x})p_d(\mathbf{x} | X)] \\ &= \mathbb{E}_{p_d(\mathbf{x} | X)} \mathbb{E}_{q_{\text{PAB}}(z | \mathbf{x})} D_{\text{KL}}[p_{\text{PAB}}(\tilde{x} | z) \parallel p_{\text{PB}}(\tilde{x} | z)] \\ &\quad + \mathbb{E}_{p_d(\mathbf{x} | X)} D_{\text{KL}}[q_{\text{PAB}}(z | \mathbf{x}) \parallel q_{\text{PB}}(z | \mathbf{x})]. \end{aligned}$$

The last term is further decomposed as

$$\begin{aligned} D_{\text{KL}}[q_{\text{PAB}}(z | \mathbf{x}) \parallel q_{\text{PB}}(z | \mathbf{x})] &= D_{\text{KL}}[q(z_P | \mathbf{x}, z_A, z_B)q(z_A | \mathbf{x})q(z_B | \mathbf{x}) \\ &\quad \parallel q(z_P | \mathbf{x}, z_B)p(z_A)q(z_B | \mathbf{x})] \\ &= \mathbb{E}_{q(z_A | \mathbf{x})q(z_B | \mathbf{x})} D_{\text{KL}}[q(z_P | \mathbf{x}, z_A, z_B) \parallel q(z_P | \mathbf{x}, z_B)] \\ &\quad + D_{\text{KL}}[q(z_A | \mathbf{x}) \parallel p(z_A)] + D_{\text{KL}}[q(z_B | \mathbf{x}) \parallel q(z_B | \mathbf{x})] \\ &= \mathbb{I}(z_P; z_A | z_B) + D_{\text{KL}}[q(z_A | \mathbf{x}) \parallel p(z_A)] \end{aligned}$$

where $\mathbb{I}(z_P; z_A | z_B)$ is the conditional mutual information. The conditional mutual information is upper bounded as

follows:

$$\begin{aligned} \mathbb{I}(z_P; z_A | z_B) &= \mathbb{E}_{q(z_A | \mathbf{x})q(z_B | \mathbf{x})} D_{\text{KL}}[q(z_P | \mathbf{x}, z_A, z_B) \parallel q(z_P | \mathbf{x}, z_B)] \\ &= \int q(z_P, z_A, z_B | \mathbf{x}) \log \frac{q(z_P | \mathbf{x}, z_A, z_B)}{q(z_P | \mathbf{x}, z_B)} dz \\ &= \int q(z_P, z_A, z_B | \mathbf{x}) \log \frac{q(z_P | \mathbf{x}, z_A, z_B)q(z_B | \mathbf{x})}{q(z_P | \mathbf{x}, z_B)q(z_B | \mathbf{x})} dz \\ &= \int q(z_P, z_A, z_B | \mathbf{x}) \log \frac{q(z_P, z_B | \mathbf{x}, z_A)}{q(z_P, z_B | \mathbf{x})} dz \\ &= \int q(z_P, z_A, z_B | \mathbf{x}) \log \frac{q(z_P, z_B | \mathbf{x}, z_A)p(z_P, z_B)}{p(z_P, z_B)q(z_P, z_B | \mathbf{x})} dz \\ &= \int q(z_P, z_B | \mathbf{x}, z_A)q(z_A | \mathbf{x}) \log \frac{q(z_P, z_B | \mathbf{x}, z_A)}{p(z_P, z_B)} dz \\ &\quad - \int q(z_P, z_B | \mathbf{x}) \log \frac{q(z_P, z_B | \mathbf{x})}{p(z_P, z_B)} dz \\ &= \mathbb{E}_{q(z_A | \mathbf{x})} D_{\text{KL}}[q(z_P, z_B | \mathbf{x}, z_A) \parallel p(z_P, z_B)] \\ &\quad - D_{\text{KL}}[q(z_P, z_B | \mathbf{x}) \parallel p(z_P, z_B)] \\ &\leq \mathbb{E}_{q(z_A | \mathbf{x})} D_{\text{KL}}[q(z_P | \mathbf{x}, z_A, z_B)q(z_B | \mathbf{x}) \parallel p(z_P)p(z_B)] \\ &= \mathbb{E}_{q(z_A | \mathbf{x})q(z_B | \mathbf{x})} D_{\text{KL}}[q(z_P | \mathbf{x}, z_A, z_B) \parallel p(z_P)] \\ &\quad + D_{\text{KL}}[q(z_B | \mathbf{x}) \parallel p(z_B)]. \end{aligned}$$

Therefore,

$$\begin{aligned} D_{\text{KL}}[p_{\text{PAB}}(\tilde{x} | X) \parallel p_{\text{PB}}(\tilde{x} | X)] &\leq \mathbb{E}_{p_d(\mathbf{x} | X)} \left[\mathbb{E}_{q_{\text{PAB}}(z | \mathbf{x})} D_{\text{KL}}[p_{\text{PAB}}(\tilde{x} | z) \parallel p_{\text{PB}}(\tilde{x} | z)] \right. \\ &\quad \left. + \mathbb{E}_{q(z_A | \mathbf{x})q(z_B | \mathbf{x})} D_{\text{KL}}[q(z_P | \mathbf{x}, z_A, z_B) \parallel p(z_P)] \right. \\ &\quad \left. + D_{\text{KL}}[q(z_B | \mathbf{x}) \parallel p(z_B)] + D_{\text{KL}}[q(z_A | \mathbf{x}) \parallel p(z_A)] \right]. \end{aligned}$$

□

B. Additional Results

We present additional experimental results including investigation of the sensitivity of hyperparameter values, ablation study on the proposed regularizers, and some observation on training runtime.

B.1. Experiments on Forced Damped Pendulum

Hyperparameter sensitivity We investigated the sensitivity of the performance with regard to the hyperparameters, i.e., the regularization coefficients, α , β , and γ . We varied them around the nominal values, i.e., the setting with which the results were reported in the main text ($\alpha = 10^{-2}$, $\beta = 10^{-1}$, and $\gamma = 10^{-3}$; see also Section C). Figure 7 summarizes the result. We can consistently observe the tendency that 1) Phys+NN with regularization is far better than Physics-only in terms of the reconstruction error (upper row); and that 2) Phys+NN with regularization is far

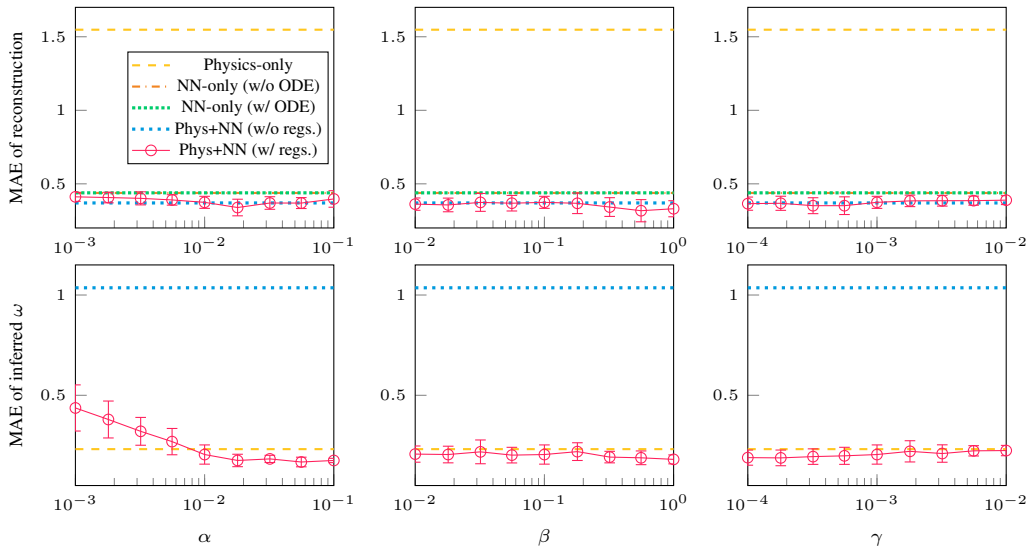


Figure 7. Performances on the pendulum data with one of the hyperparameters (α , β , or γ) varied around the nominal value, while the others maintained. Averages and SDs over five random trials are reported. Reference values are shown in dashed or dotted lines.

Table 3. Ablation study on the pendulum data. Averages (and SDs) over 20 random trials are reported.

| | MAE of reconstruction | | MAE of inferred ω | |
|---|-----------------------|------------------------|--------------------------|------------------------|
| No R_{PPC} (i.e., $\alpha = 0$) | 0.396 | (4.3×10^{-2}) | 0.889 | (1.9×10^{-1}) |
| No R_{GP} (i.e., $\beta = 0$) | 0.381 | (4.1×10^{-2}) | 0.276 | (4.2×10^{-2}) |
| No R_U (i.e., $\gamma = 0$) | 0.372 | (4.1×10^{-2}) | 0.223 | (3.6×10^{-2}) |
| With all regularizers | 0.363 | (4.8×10^{-2}) | 0.229 | (3.8×10^{-2}) |

Table 4. Performances on test set of the advection-diffusion data. Averages (and SDs) over 20 random trials are reported.

| | MAE of reconstruction | | MAE of inferred a | |
|--------------------|-----------------------|------------------------|---------------------|------------------------|
| Physics-only | 0.393 | (9.5×10^{-4}) | 0.0103 | (1.5×10^{-3}) |
| NN-only, w/o PDE | 0.0396 | (2.2×10^{-4}) | – | – |
| NN-only, w/ PDE | 0.0388 | (1.7×10^{-4}) | – | – |
| Phys+NN, w/o regs. | 0.0404 | (1.2×10^{-2}) | 0.258 | (3.2×10^{-1}) |
| Phys+NN, w/ regs. | 0.0437 | (1.5×10^{-3}) | 0.00951 | (6.2×10^{-3}) |

better than Phys+NN without regularization in terms of the estimation error of physics parameter ω (lower row).

Ablation study We performed an ablation study where either of the proposed three regularizers was turned off (i.e., one of the three coefficients, α , β , and γ is fixed to be 0, and the remaining ones were set to be the nominal values). Table 3 summarizes the result. We can observe the importance of the presence of *every* regularizer; if one of them is missing, the reconstruction performance and/or the physics parameter estimation deteriorate.

Training runtime In training, the NN-only model took about 5.13 seconds for 10 epochs, and the Phys+NN model with regularization took about 10.9 seconds for 10 epochs, though we believe our implementation can still be improved for more efficiency. The difference probably stems from the physics-part encoder.

B.2. Experiments on Advection-Diffusion System

Reconstruction and estimation errors In Table 4, we show the error statistics of the reconstruction and estimation of the physics parameter a on the test set, which were

omitted from the main text.

Hyperparameter sensitivity We investigated the sensitivity of the performance with regard to the hyperparameters α , β , and γ . We varied these values around the nominal values, i.e., the setting with which the results were reported in the main text ($\alpha = 10^{-1}$, $\beta = 10^6$, and $\gamma = 10^{-2}$; see also hyperparameter settings in Section C). Figure 8 summarizes the result. Across all the coefficient values, we can consistently observe the tendency similar to that in the pendulum data experiment.

Ablation study We performed an ablation study where either of the proposed three regularizers was turned off. Table 5 summarizes the result, with which we can observe the importance of the presence of every regularizer similarly to the pendulum data experiment.

Training runtime In training, the NN-only model took about 6.01 seconds for 10 epochs, and the Phys+NN model with regularization took about 15.4 seconds for 10 epochs.

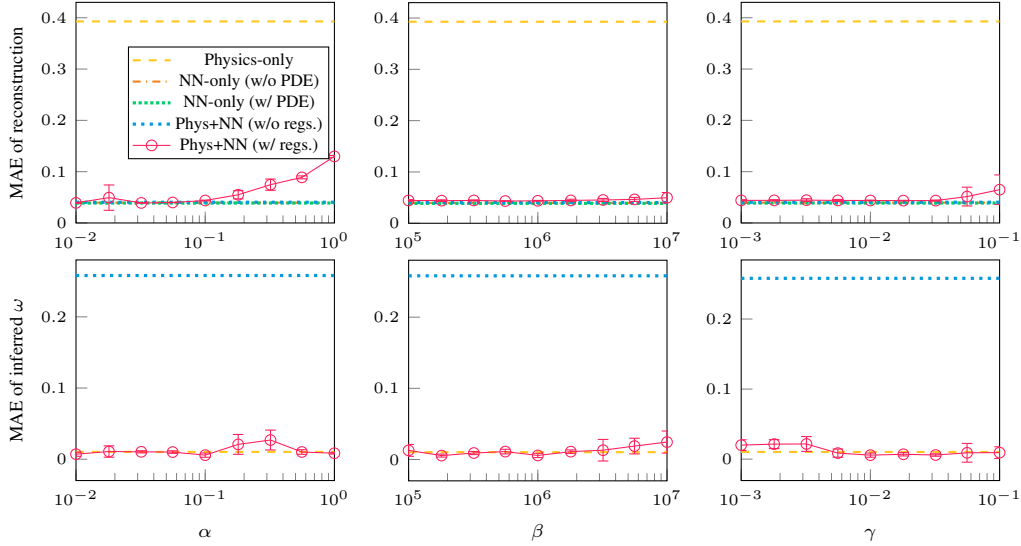


Figure 8. Performances on the advection-diffusion data with one of the hyperparameters (α , β , or γ) varied around the nominal value, while the others maintained. Averages and SDs over five random trials are reported. Reference values are shown in dashed or dotted lines.

Table 5. Ablation study on the advection-diffusion data. Averages (and SDs) over 20 random trials are reported.

| | MAE of reconstruction | | MAE of inferred a | |
|---|-----------------------|--------------------------|---------------------|--------------------------|
| No R_{PPC} (i.e., $\alpha = 0$) | 0.0461 | (1.3×10^{-2}) | 0.0444 | (1.4×10^{-2}) |
| No R_{g_P} (i.e., $\beta = 0$) | 0.0588 | (9.1×10^{-4}) | 0.0548 | (9.4×10^{-7}) |
| No R_U (i.e., $\gamma = 0$) | 0.0747 | (2.4×10^{-2}) | 0.199 | (2.3×10^{-1}) |
| With all regularizers | 0.0437 | (1.5×10^{-3}) | 0.00951 | (6.2×10^{-3}) |

Table 6. Performances on test set of the galaxy image data. Averages (and SDs) over the whole test set are reported.

| | MAE of reconstruction | |
|-----------------------|-----------------------|--------------------------|
| Physics-only | 0.0264 | (3.9×10^{-2}) |
| NN-only | 0.0167 | (3.0×10^{-2}) |
| Phys+NN, $\alpha = 0$ | 0.0188 | (3.4×10^{-2}) |
| Phys+NN, $\alpha > 0$ | 0.0180 | (3.3×10^{-2}) |

B.3. Experiments on Galaxy Images

Reconstruction In Figure 9, we show examples of reconstruction of five test samples. While the Physics-only model cannot recover the color information by construction, the other models that include neural nets reproduce the original colors to some extent. The reconstruction errors over the whole test set are reported in Table 6. From these results, we can observe that the reconstruction performance is similar between the NN-only model and the Phys+NN models. Despite the similar reconstruction performance, the Phys+NN model with the regularization achieves clearly better generation performance as shown in the main text.

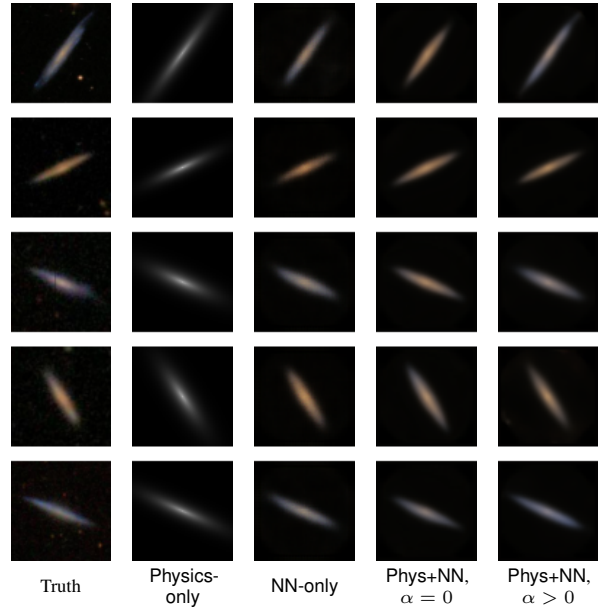


Figure 9. Examples of reconstruction of five test samples of the galaxy image data. Best viewed in color.

Counterfactual generation In Figure 10, we show the result of generation, where we varied the last element of \mathbf{z}_P that corresponds to the angle of a galaxy in image, θ . We examined the models trained without or with one of the regularizers, R_{PPC} (i.e., $\alpha = 0$); the other regularizers were always active. In Figure 10, the case without the regularizer does not show reasonable generation with different θ . Note that $\theta < 0$ was never encountered during training as we set the range of the last element of \mathbf{z}_P to be non-negative; nevertheless reasonable images are generated with $\theta < 0$.

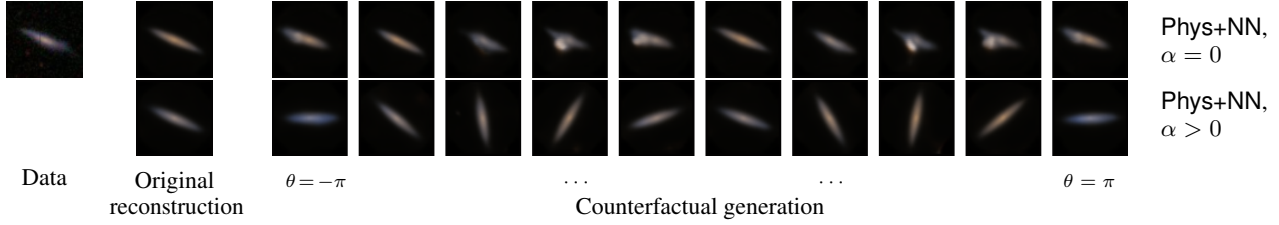


Figure 10. Counterfactual generation for the galaxy image data. (left) Original data sample. (center) Original reconstruction of the sample. (right) Generation with varying $[z_P]_4$, which corresponds to the angle of galaxy in an image, θ , from $-\pi$ to π .

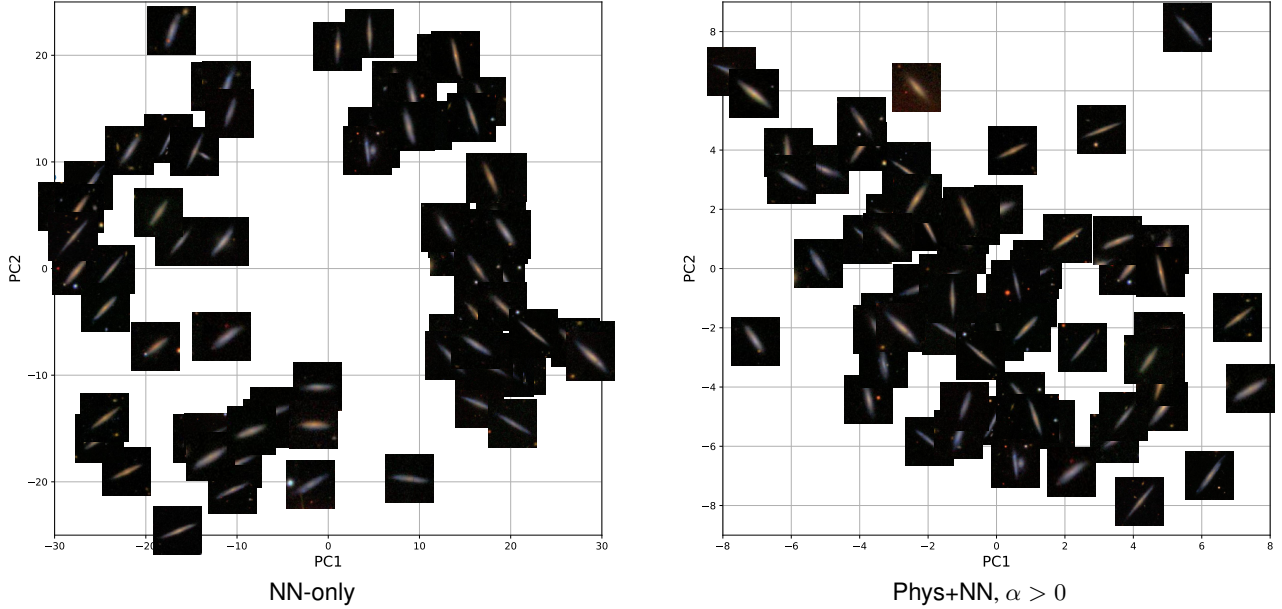


Figure 11. Visualization of latent variable z_B learned from the galaxy image data. The corresponding test data samples are shown at the points specified by the first two principal scores of z_B .

Latent variable z_B We computed the first two principal scores of z_B and plotted them with the corresponding image sample in Figure 11. In the NN-only model, the distribution of z_B clearly corresponds to the angle of the galaxy in images. In contrast in the Phys+NN model, such a correspondence is not observed. This is a reasonable result because in the Phys+NN model, the semantic of galaxy angle is completely assigned to the last element of z_P .

C. Details of Experiments

C.1. Infrastructure

We implemented the models using Python 3.8.0 with PyTorch 1.7.0 and NumPy 1.19.2 throughout the experiments. We used SciPy of version 1.5.2 in generating the synthetic datasets.

The computation was performed with a machine equipped with an NVIDIA[®] Tesla[™] V100 GPU in the experiment on

the galaxy images dataset. We used a machine equipped with a CPU of Intel[®] Xeon[®] Gold 6148 in the other experiments.

C.2. Experiments on Forced Damped Pendulum Data

Data-generating process We consider a gravity pendulum with damping effect and external force. Let $\theta(t)$ be the angle of the pendulum at time t . We generated the data by numerically integrating an ODE:

$$\frac{d^2\theta(t)}{dt^2} + \omega^2 \sin \theta(t) + \gamma \frac{d\theta(t)}{dt} - A\omega^2 \cos(2\pi\phi t) = 0,$$

using `scipy.integrate.solve_ivp` with the explicit Runge–Kutta method of order 8. The tolerance parameters `rtol` and `atol` were kept to be the default values, 10^{-3} and 10^{-6} , respectively. We evaluated the solution's values at timesteps $t = 0, \Delta t, \dots, (\tau - 1)\Delta t$ with $\Delta t = 0.05$ and $\tau = 50$ using the 7-th order interpolation polynomial. The values of the parameters, ω, γ, A ,

and ϕ , as well as the initial condition $\theta(0)$ were randomly sampled when creating each sequence. The random sampling was with the uniform distributions on the following ranges: $\omega \in [0.785, 3.14]$, $\gamma \in [0, 0.8]$, $f \in [3.14, 6.28]$, $A \in [0, 40]$, and $\theta(0) \in [-1.57, 1.57]$. The initial condition of $\dot{\theta}(0)$ was fixed to be 0. Each element of each generated sequence was added by zero-mean Gaussian noise with standard deviation 0.01.

Data property The overall dataset we generated comprises 3,500 elements (data-points) in total. Each data-point \mathbf{x} is a sequence of length τ of pendulum’s angle, that is,

$$\mathbf{x}_i = [\theta_i(0) \theta_i(\Delta t) \cdots \theta_i((\tau - 1)\Delta t)]^T \in \mathbb{R}^\tau,$$

where $i = 1, \dots, 3500$ is the sample index.

Train/valid/test split We first extracted 500 and 1,000 sequences randomly from the overall dataset as the validation set and the test set, respectively. We then selected 1,000 sequences out of the remaining 2,000 sequences to make a training set. This selection was randomly done every time; so a different random seed resulted in a different training set.

Physics model A part of the data-generating process was given as physics model: $f_P(\theta, z_P) = \ddot{\theta} + z_P \sin \theta$.

Latent variables By construction of f_P , $z_P \in \mathbb{R}$ is expected to work in the same manner as ω^2 in the data-generating process. There were also $z_A \in \mathbb{R}$ and $z_B \in \mathbb{R}^2$ in the full Phys+NN model. Meanwhile, we used $z_B \in \mathbb{R}^4$ (and no z_A, z_P) in the NN-only model without ODE; and $z_A \in \mathbb{R}^2$ and $z_B \in \mathbb{R}^2$ (and no z_P) in the NN-only model with ODE.

Decoder architecture We describe the decoder architecture of the full Phys+NN model. In the first stage, \mathcal{S} , an ODE $f_P(\theta, z_P) + f_A(\theta, z_A) = 0$ is numerically solved with the Euler method for length τ with step size Δt . Let $\nu_{PA} \in \mathbb{R}^\tau$ be the output of \mathcal{S} , i.e., the solution sequence. In the second stage, \mathcal{M} , ν_{PA} is then augmented with the output of $f_B(z_B)$, i.e., $\mu_{PAB} = \nu_{PA} + f_B(z_B)$. We modeled f_A with a multilayer perceptron (MLP) with two hidden layers of size 64. We modeled f_B also with an MLP with two hidden layers of size 128. We used the exponential linear unit (ELU) with $\alpha = 1.0$ as activation function after the hidden layers.

Encoder architecture We describe the encoder architecture of the full Phys+NN model. We modeled each of the recognition networks, g_A , g_B , and g_P , with an MLP with five hidden layers of size 128, 128, 256, 64, and 32. We modeled U as $U(\mathbf{x}, z_A, z_B) = \mathbf{x} + U'(\mathbf{x}, z_A, z_B)$, where U' was an MLP with two hidden layers of size 128. We used ELU with $\alpha = 1.0$ as activation function after the hidden layers. We put a softplus function after the final output of g_P to make its output positive-valued.

Replacement functions To create the reduced models, we replaced f_A and f_B respectively by $h_A = 0$ and $h_B = 0$. This choice of the replacers is reasonable because both f_A and f_B appear in the additive form.

Hyperparameters We selected the hyperparameters, α , β , and γ , from the following sets: $\alpha \in \{10^{-3}, 10^{-2}, 10^{-1}\}$, $\beta \in \{10^{-2}, 10^{-1}, 1\}$, and $\gamma \in \{10^{-4}, 10^{-3}, 10^{-2}\}$. These ranges were chosen to roughly adjust the values of the corresponding regularizers to that of the ELBO. The configuration that achieved the best reconstruction error on the validation set was selected finally: $\alpha = 10^{-2}$, $\beta = 10^{-1}$, and $\gamma = 10^{-3}$. In computing R_{g_P} , we sampled z_P from the uniform distribution on range $[0.392, 3.53]$.

Optimization We used the Adam optimizer with $\alpha = 10^{-3}$, $\beta_1 = 0.9$, $\beta_2 = 0.999$, and $\epsilon = 10^{-3}$. We ran iterations with mini-batch size 200 for 5000 epochs (i.e., 25,000 iterations in total) and saved the model that achieved the best validation reconstruction error.

C.3. Experiments on Advection-Diffusion System

Data-generating process We consider the advection (convection) and diffusion of something (e.g., heat) on the 1-dimensional space, which is described by the following PDE:

$$\frac{\partial T(t, s)}{\partial t} - a \frac{\partial^2 T(t, s)}{\partial s^2} + b \frac{\partial T(t, s)}{\partial s} = 0,$$

where t and s denote the time and space dimension, respectively. We numerically solved this PDE using `scipy.integrate.solve_ivp` with the explicit Runge–Kutta method of order 8. The spatial derivative was computed with discretization on the H -point even grid between $s = 0$ and $s = s_{\max}$ with $H = 12$ and $s_{\max} = 2$. We evaluated the solutions values at timesteps $t = 0, \Delta t, \dots, (\tau - 1)\Delta t$ with $\Delta t = 0.02$ and $\tau = 50$. The initial condition was set $T(0, s) = c \sin(\pi s / s_{\max})$, and we set the Dirichlet boundary condition $T(t, 0) = T(t, s_{\max}) = 0$. The values of the parameters a , b , and c were randomly sampled when creating each sequence. The random sampling was with the uniform distributions on the following ranges: $a \in [10^{-2}, 10^{-1}]$, $b \in [10^{-2}, 10^{-1}]$, and $c \in [0.5, 1.5]$. Each element of each generated sequence was added by zero-mean Gaussian noise with standard deviation 0.001.

Data property The overall dataset we generated comprises 3,500 sequences, each of which is

$$\mathbf{x}_i = \begin{bmatrix} T_i(0, 0) & T_i(\Delta t, 0) & \cdots & T_i((\tau - 1)\Delta t, 0) \\ \vdots & \vdots & & \vdots \\ T_i(0, s_{\max}) & T_i(\Delta t, s_{\max}) & \cdots & T_i((\tau - 1)\Delta t, s_{\max}) \end{bmatrix} \in \mathbb{R}^{H \times \tau}.$$

Train/valid/test split We first extracted 500 and 1,000 sequences randomly from the overall dataset as the validation set and the test set, respectively. We then selected 1,000 sequences out of the remaining 2,000 sequences to make a training set. This selection was randomly done every time; so a different random seed resulted in a different training set.

Physics model A part of the data-generating process was given as physics model: $f_P(T, z_P) = T_t - z_P T_{ss}$.

Latent variables By construction of f_P , $z_P \in \mathbb{R}$ is expected to work in the same manner as a in the data-generating process. There was also $z_A \in \mathbb{R}^4$ (and no z_B) in the full Phys+NN model. Meanwhile, we used $z_B \in \mathbb{R}^5$ (and no z_A, z_P) in the NN-only model without PDE; and $z_A \in \mathbb{R}^5$ (and no z_B, z_P) in the NN-only model with PDE.

Decoder architecture We describe the decoder architecture of the full Phys+NN model. In \mathcal{S} , a PDE $f_P(T, z_P) + f_A = 0$ was numerically solved with the finite difference method with the explicit scheme for length τ with temporal step size Δt . Meanwhile, \mathcal{M} does nothing as there is no B-part. We modeled f_A with an MLP with two hidden layers of size 64. We used ELU with $\alpha = 1.0$ as activation function after the hidden layers.

In the NN-only model without PDE, we modeled f_B with an MLP with a hidden layer of size 128.

Encoder architecture We describe the encoder architecture of the full Phys+NN model. We modeled each of the recognition networks, g_A and g_P , with an MLP with five hidden layers of size 256, 256, 256, 64, and 32. We modeled $U(\mathbf{x}, z_A, z_B)$ with an MLP with two hidden layers of size 256. We used ELU with $\alpha = 1.0$ as activation function after the hidden layers. We put a softplus function after the final output of g_P to make its output positive-valued.

Replacement functions To create the reduced model, we replaced f_A by $h_A = 0$.

Hyperparameters We selected the hyperparameters, α , β , and γ , from the following sets: $\alpha \in \{10^{-2}, 10^{-1}\}$, $\beta \in \{10^5, 10^6\}$, and $\gamma \in \{10^{-2}, 10^{-1}\}$. These ranges were chosen to roughly adjust the values of the corresponding regularizers to that of the ELBO. The configuration that achieved the best reconstruction error on the validation set was selected finally: $\alpha = 10^{-1}$, $\beta = 10^6$, and $\gamma = 10^{-2}$. In computing R_{g_P} , we sampled z_P from the uniform distribution on range $[0.005, 0.2]$.

Optimization We used the Adam optimizer with $\alpha = 10^{-3}$, $\beta_1 = 0.9$, $\beta_2 = 0.999$, and $\epsilon = 10^{-3}$. We ran iterations with mini-batch size 200 for 20000 epochs (i.e., 100,000 iterations in total) and saved the model that achieved the best validation reconstruction error.

C.4. Experiments on Galaxy Images

Physics model The physics model $f_P: \mathbb{R}^4 \rightarrow \mathbb{R}^{69 \times 69}$ is an exponential profile of the light distribution of galaxies whose input is $z_P = [I_0 \ A \ B \ \theta]^T \in \mathbb{R}_{>0}^4$, whose elements have the semantics introduced in the following. Let $[f_P]_{i,j}$ denote the (i, j) -element of the output of f_P . Then, for $1 \leq i, j \leq 69$,

$$[f_P]_{i,j} = I_0 \exp(-r_{i,j}),$$

where

$$r_{i,j}^2 = \frac{(X_j \cos \theta - Y_i \sin \theta)^2}{A^2} + \frac{(X_j \sin \theta + Y_i \cos \theta)^2}{B^2},$$

$$X_j = 2(j-1)/68 - 1, \quad Y_i = -2(i-1)/68 + 1.$$

(X_j, Y_i) is the coordinate on the 69×69 even grid on $[-1, 1] \times [-1, 1]$. I_0 determines the overall magnitude of the light distribution, A and B determine the size of the ellipse of the light distribution, and θ determines its rotation. This model was used in a similar problem of Aragon-Calvo and Carvajal (2020), where they only handle artificial images.

Latent variables $z_P \in \mathbb{R}^4$ is as described above. In addition, we used $z_B \in \mathbb{R}^2$ (and no z_A) in the full Phys+NN model. Meanwhile, we used $z_B \in \mathbb{R}^4$ (and no z_A, z_P) in the NN-only model.

Decoder architecture In the Phys+NN model, \mathcal{S} is just a function evaluation, i.e., $\nu_P = \mathcal{S}[z_P; f_P] = f_P(z_P) \in \mathbb{R}^{69 \times 69}$. In \mathcal{M} , we compute

$$\mathcal{M}[\nu_P, z_B; f_{B, \text{Unet}}, f_{B, \text{tconv}}]$$

$$= f_{B, \text{Unet}}(\nu_P, f_{B, \text{tconv}}(z_B)).$$

$f_{B, \text{tconv}}$ is a neural net with transposed convolutional layers and given z_B , outputs a signal in $\mathbb{R}^{69 \times 69}$. $f_{B, \text{Unet}}$ is a neural net with architecture similar to the U-Net, whose outputs are in $\mathbb{R}^{69 \times 69 \times 3}$. We used the rectified linear unit (ReLU) as activation function and applied batch normalization before each activation function.

In the NN-only model, we modeled $f_B(z_B)$ only with a neural net with transposed convolutional layers whose output is in $\mathbb{R}^{69 \times 69 \times 3}$.

Encoder architecture The architecture of g_P and g_B is similar to the one in Aragon-Calvo and Carvajal (2020). We put the softplus function after the final output of g_P to make its output positive-valued. U is simply $U(\mathbf{x}) = \sum_{i=1}^3 c_i [\mathbf{x}]_i$, where $[\mathbf{x}]_i$ denotes the i -th channel of \mathbf{x} , and c 's are trainable parameters.

Replacement functions To create the reduced model, we replaced $f_{B, \text{Unet}}$ by h_B such that $h_B(\nu_P) = [\nu_P; \nu_P; \nu_P] \in \mathbb{R}^{69 \times 69 \times 3}$.

Hyperparameters We selected the hyperparameter α from $\alpha \in \{10^{-2}, 10^{-1}, 1\}$. This range was chosen to roughly adjust the value of the corresponding regularizer to that of the ELBO. The other hyperparameters were fixed to be $\beta = 10^3$ and $\gamma = 1$; these values were also determined by roughly adjusting the order of the values of objectives. In computing R_{gp} , we sampled from the uniform distributions on $I_0 \in [0.5, 1]$, $A \in [0.1, 1.0]$, $e \in [0.2, 0.8]$, and $\theta \in [0, 3.142]$, where $B = A(1 - e)$.

C.5. Experiments on Human Locomotion

Physics model We modeled f_P with a trainable Hamilton’s equation as in Toth et al. (2020); Greydanus et al. (2019):

$$f_P \left(\begin{bmatrix} \mathbf{p}^\top & \mathbf{q}^\top \end{bmatrix}^\top, \mathbf{z}_P \right) = \begin{bmatrix} -\frac{\partial \mathcal{H}}{\partial \mathbf{q}}^\top & \frac{\partial \mathcal{H}}{\partial \mathbf{p}}^\top \end{bmatrix}^\top, \quad (26)$$

where $\mathbf{p} \in \mathbb{R}^{d_y}$ is a generalized position, $\mathbf{q} \in \mathbb{R}^{d_y}$ is a generalized momentum, and $\mathcal{H}: \mathbb{R}^{d_y} \times \mathbb{R}^{d_y} \rightarrow \mathbb{R}$ is a Hamiltonian. We let $d_y = 3$ and modeled \mathcal{H} with an MLP with two hidden layers of size .

Latent variables $\mathbf{z}_P \in \mathbb{R}^{2d_y}$ is used as the initial condition of \mathbf{p} and \mathbf{q} . There was also $\mathbf{z}_B \in \mathbb{R}^{15}$.

Decoder architecture In the full Phys+NN model, \mathcal{S} is a numerical solver of ODE $f_P = 0$ with the Euler method. Its output is then transformed by f_B , an MLP with two hidden layers of size 512.

Encoder architecture g_P and g_B are MLPs with five hidden layers of size 512, 512, 512, 64, 32.

Replacement functions To create the reduced model, we replaced f_B by a linear function h_B , where h_B is applied to each snapshot of a sequence independently.

Hyperparameters We selected the hyperparameter α from $\alpha \in \{10^{-3}, 10^{-2}, 10^{-1}, 1\}$. This range was chosen to roughly adjust the value of the corresponding regularizer to that of the ELBO. The other hyperparameters were just $\beta = \gamma = 0$ as we did not use the corresponding regularizers.

D. Architecture Examples from Literature

We exemplify some architectures of physics-integrated machine learning models. Most of the studies referred to here did not aim generative modeling originally, though the ideas can be fitted to our general architecture of physics-integrated VAEs. Below we assume $k_P = k_A = k_B = 1$ unless f has a numbering subscript.

One of the most prevailing forms of \mathcal{S} is a numerical solver of dynamics models such as ODEs, PDEs, and discrete-time difference equations. In such a case, f_P and f_A give the terms that appear in a dynamics equation. They are combined additively in many cases (Rico-Martínez et al., 1994;

Thompson and Kramer, 1994; Reinhart et al., 2017; Golemo et al., 2018; Mehta et al., 2020; Déchelle et al., 2020; Roehrl et al., 2020; Le Guen and Thome, 2020; Le Guen et al., 2021; Viana et al., 2021), that is,

$$\mathcal{S} = \text{solve}_y [f_P(y, \mathbf{z}_P) + f_A(y, \mathbf{z}_A) = 0], \quad (27)$$

where solve_y refers to a numerical ODE/PDE solver with regard to y and returns the value of the solution on some time/space grid.

Another way of combining f_P and f_A is the composition (Psychogios and Ungar, 1992; Thompson and Kramer, 1994; Long and She, 2018; Wan et al., 2018; Lanusse et al., 2019; de Bézenac et al., 2019; Mohan et al., 2020; Matei et al., 2020; Behjat et al., 2020; Arık et al., 2020; Li et al., 2020; Jiang et al., 2021), that is,

$$\mathcal{S} = \text{solve}_y [f_P(y, \mathbf{z}_P, f_A(y, \mathbf{z}_A)) = 0], \quad (28)$$

where f_A often gives estimation of some unknown or varying physics parameters in f_P . The order of the composition may reverse in some studies (Ajay et al., 2018; 2019), that is,

$$\mathcal{S} = \text{solve}_y [f_A(y, \mathbf{z}_A, f_P(y, \mathbf{z}_P)) = 0], \quad (29)$$

where the output of physics model is corrected by machine learning (so-called residual physics). Some studies consider more complex combinations of f_P and f_A , for example, $\mathcal{S} = \text{solve}[f_{P,2}(f_A(f_{P,1})) = 0]$ (Raissi, 2018; De Groot et al., 2019; Heiden et al., 2020; Kaltenbach and Koutsourakakis, 2021). A trickier case appears in Jiang et al. (2018), where discrete state of contact dynamics is first determined by a data-driven classifier, which is then used for choosing one of physics models (also including learnable ones) to be used.

We note that \mathcal{S} is not necessarily an ODE/PDE solver. If (augmented) physics models are algebraic equations with closed-form solutions, \mathcal{S} just works as a function evaluation (e.g., Aragon-Calvo and Carvajal, 2020). If no closed-form solution is available, a differentiable optimizer may be utilized in \mathcal{S} .

Another functional, \mathcal{M} , performs just function evaluations in most cases, while there are some variations in how f_B and the output of \mathcal{S} are wired. Let \mathbf{y} denote the output of \mathcal{S} regardless of the inside of \mathcal{S} . The most straightforward and popular form is $\mathcal{M} = f_B(\mathbf{y}, \mathbf{z}_B)$. Some other meticulously designed forms include $\mathcal{M} = f_B(\mathbf{y}, \mathbf{z}_B) + \mathbf{y}$, $\mathcal{M} = f_{B,2}(f_{B,1}, \mathbf{y})$, and $\mathcal{M} = \sum_i f_{B,i} \cdot \mathbf{y}_i$. There are several kinds of intention in the use of f_B , such as:

- f_B corrects the physics-based output \mathbf{y} to compensate inaccuracy of physics models or unmodeled phenomena (Young et al., 2017; Chen et al., 2018b; Nutkiewicz et al., 2018; Singh et al., 2019; Wang et al., 2019; Zeng et al., 2019);

- physics-based output \mathbf{y} is used as input features of machine learning model (Karpatne et al., 2017b; Pawar et al., 2020; Muralidhar et al., 2020; Zhang et al., 2021; Belbute-Peres et al., 2020);
- f_B works as an observation function that changes signal’s modality (Greydanus et al., 2019; Lutter et al., 2019; Yıldız et al., 2019; Linial et al., 2020; Toth et al., 2020; Cranmer et al., 2020; Saemundsson et al., 2020); and
- f_B works as a learnable ensemble of physics models (Sengupta et al., 2020).

We refer to the excellent survey / overview papers for more information (Thompson and Kramer, 1994; Karpatne et al., 2017a; Ren et al., 2018; Wang et al., 2019; Camps-Valls et al., 2020; Shlezinger et al., 2020; Willard et al., 2020; Schölkopf et al., 2021). We also refer to the idea of neural architecture search in this context (Ba et al., 2019).

E. Extensions

While the proposed framework is useful as shown in our experiments, there are several directions to go for possible technical improvement of the method. First, physics-integrated VAEs can be further combined with techniques to solve ODEs and PDEs with neural networks (Raissi et al., 2019; Yang and Perdikaris, 2018; Yang et al., 2021). We supposed the use of differentiable numerical solvers if \mathcal{S} contain ODEs or PDEs, but such numerical solvers are often computationally heavy. Replacing them with neural net-based solutions will be useful for various applications. Second, while we defined the regularizer based on the (possibly loose) upper bound of KL divergence, we may use other dissimilarity measure of distributions or random variables, such as maximum mean discrepancy. Third, in a special case where $k_A = 0$ and f_B is an invertible model, U can be replaced by the inverse, f_B^{-1} . Lastly, the proposed regularization method can be extended to other types of deep generative models; e.g., an extension to InfoVAE (Zhao et al., 2019) is straightforward.